COMILLAS
UNIVERSIDAD PONTIFICIA
ICAI

GRADO EN INGENIERÍA EN TECNOLOGÍAS INDUSTRIALES

TRABAJO FIN DE GRADO

CONCEPTUAL DESIGN OF COMPACT HEAT EXCHANGER TECHNOLOGY FOR HYDROGEN FUELED AIRCRAFT

Autor: Pedro Ureña Álvarez

Director: Carlos Xisto

Co-Director: Isak Jonsson

Madrid

Declaro, bajo mi responsabilidad, que el Proyecto presentado con el título

Conceptual design of compact heat exchanger technology for hydrogen fueled aircraft

en la ETS de Ingeniería - ICAI de la Universidad Pontificia Comillas en el

curso académico 2020/21 es de mi autoría, original e inédito y

no ha sido presentado con anterioridad a otros efectos.

El Proyecto no es plagio de otro, ni total ni parcialmente y la información que ha sido

tomada de otros documentos está debidamente referenciada.

Fdo.: Pedro Ureña Álvarez Fecha: 29 / 06 / 2021

Autorizada la entrega del proyecto

EL DIRECTOR DEL PROYECTO

Fdo.: Carlos Xisto Fecha: 30 / 06 / 2021

AUTORIZACIÓN PARA LA DIGITALIZACIÓN, DEPÓSITO Y DIVULGACIÓN EN RED DE PROYECTOS FIN DE GRADO, FIN DE MÁSTER, TESINAS O MEMORIAS DE BACHILLERATO

1º. Declaración de la autoría y acreditación de la misma.

El autor D._____Pedro Ureña Álvarez_____
DECLARA ser el titular de los derechos de propiedad intelectual de la obra: __Conceptual design of compact heat exchanged technology for hydrogen fueled aircraft_, que ésta es una obra original, y que ostenta la condición de autor en el sentido que otorga la Ley de Propiedad Intelectual.

2º. Objeto y fines de la cesión.

Con el fin de dar la máxima difusión a la obra citada a través del Repositorio institucional de la Universidad, el autor **CEDE** a la Universidad Pontificia Comillas, de forma gratuita y no exclusiva, por el máximo plazo legal y con ámbito universal, los derechos de digitalización, de archivo, de reproducción, de distribución y de comunicación pública, incluido el derecho de puesta a disposición electrónica, tal y como se describen en la Ley de Propiedad Intelectual. El derecho de transformación se cede a los únicos efectos de lo dispuesto en la letra a) del apartado siguiente.

3º. Condiciones de la cesión y acceso

Sin perjuicio de la titularidad de la obra, que sigue correspondiendo a su autor, la cesión de derechos contemplada en esta licencia habilita para:

a) Transformarla con el fin de adaptarla a cualquier tecnología que permita incorporarla a internet y hacerla accesible; incorporar metadatos para realizar el registro de la obra e incorporar "marcas de agua" o cualquier otro sistema de seguridad o de protección.
b) Reproducirla en un soporte digital para su incorporación a una base de datos electrónica, incluyendo el derecho de reproducir y almacenar la obra en servidores, a los efectos de garantizar su seguridad, conservación y preservar el formato.
c) Comunicarla, por defecto, a través de un archivo institucional abierto, accesible de modo libre y gratuito a través de internet.
d) Cualquier otra forma de acceso (restringido, embargado, cerrado) deberá solicitarse expresamente y obedecer a causas justificadas.
e) Asignar por defecto a estos trabajos una licencia Creative Commons.
f) Asignar por defecto a estos trabajos un HANDLE (URL *persistente)*.

4º. Derechos del autor.

El autor, en tanto que titular de una obra tiene derecho a:

a) Que la Universidad identifique claramente su nombre como autor de la misma
b) Comunicar y dar publicidad a la obra en la versión que ceda y en otras posteriores a través de cualquier medio.
c) Solicitar la retirada de la obra del repositorio por causa justificada.
d) Recibir notificación fehaciente de cualquier reclamación que puedan formular terceras personas en relación con la obra y, en particular, de reclamaciones relativas a los derechos de propiedad intelectual sobre ella.

5º. Deberes del autor.

El autor se compromete a:

a) Garantizar que el compromiso que adquiere mediante el presente escrito no infringe ningún derecho de terceros, ya sean de propiedad industrial, intelectual o cualquier otro.
b) Garantizar que el contenido de las obras no atenta contra los derechos al honor, a la intimidad y a la imagen de terceros.
c) Asumir toda reclamación o responsabilidad, incluyendo las indemnizaciones por daños, que pudieran ejercitarse contra la Universidad por terceros que vieran infringidos sus derechos e intereses a causa de la cesión.

d) Asumir la responsabilidad en el caso de que las instituciones fueran condenadas por infracción de derechos derivada de las obras objeto de la cesión.

6º. Fines y funcionamiento del Repositorio Institucional.

La obra se pondrá a disposición de los usuarios para que hagan de ella un uso justo y respetuoso con los derechos del autor, según lo permitido por la legislación aplicable, y con fines de estudio, investigación, o cualquier otro fin lícito. Con dicha finalidad, la Universidad asume los siguientes deberes y se reserva las siguientes facultades:

- La Universidad informará a los usuarios del archivo sobre los usos permitidos, y no garantiza ni asume responsabilidad alguna por otras formas en que los usuarios hagan un uso posterior de las obras no conforme con la legislación vigente. El uso posterior, más allá de la copia privada, requerirá que se cite la fuente y se reconozca la autoría, que no se obtenga beneficio comercial, y que no se realicen obras derivadas.
- La Universidad no revisará el contenido de las obras, que en todo caso permanecerá bajo la responsabilidad exclusive del autor y no estará obligada a ejercitar acciones legales en nombre del autor en el supuesto de infracciones a derechos de propiedad intelectual derivados del depósito y archivo de las obras. El autor renuncia a cualquier reclamación frente a la Universidad por las formas no ajustadas a la legislación vigente en que los usuarios hagan uso de las obras.
- La Universidad adoptará las medidas necesarias para la preservación de la obra en un futuro.
- La Universidad se reserva la facultad de retirar la obra, previa notificación al autor, en supuestos suficientemente justificados, o en caso de reclamaciones de terceros.

Madrid, a 29 de JUNIO de 2021

ACEPTA

Fdo. Pedro Ureña Álvarez

Motivos para solicitar el acceso restringido, cerrado o embargado del trabajo en el Repositorio Institucional:

COMILLAS
UNIVERSIDAD PONTIFICIA
ICAI

GRADO EN INGENIERÍA EN TECNOLOGÍAS INDUSTRIALES

TRABAJO FIN DE GRADO

CONCEPTUAL DESIGN OF COMPACT HEAT EXCHANGER TECHNOLOGY FOR HYDROGEN FUELED AIRCRAFT

Autor: Pedro Ureña Álvarez

Director: Carlos Xisto

Co-Director: Isak Jonsson

Madrid

DISEÑO CONCEPTUAL DE TECNOLOGÍA COMPACTA DE INTERCAMBIADOR DE CALOR PARA AVIONES DE COMBUSTIBLE CON HIDRÓGENO

Autor: Ureña Álvarez, Pedro.
Director: Xisto, Carlos.
Entidad Colaboradora: ICAI – Universidad Pontificia Comillas.

RESUMEN DEL PROYECTO

Este proyecto es un estudio de transferencia de calor sobre una paleta estructural en un ICD (Conducto Interconector). El flujo de trabajo se basa en tener antecedentes de CFD (Mecánica de Fluidos Computacional), tener una visión general de los modelos de turbulencia, validar el modelo de turbulencia a través de la verificación de placa plana y simular el caso principal.

Palabras clave: CFD, Transferencia de calor, Aire, Hidrógeno, ANSYS, CFX.

1. Introducción

Este proyecto se lleva a cabo como consecuencia de intentar predecir el Coeficiente de Transferencia de Calor en el STRUT; y también acercarnos a la comprensión de los sistemas de fluidos en los intercambiadores de calor cuando la diferencia de temperatura es significativa entre la corriente libre y la temperatura de la pared, sobre todo cuando se trabaja en condiciones de baja temperatura (<100K) y con gran diferencia térmica (300). HTC se calculará ejecutando simulaciones en el modelo 3D y una verificación de placa plana en Ansys CFX 2021 R1 [1]; Además, se comparará con correlaciones numéricas con la ayuda de MATLAB R2019b [2] y Python 3 [3] con otras bibliotecas. Durante la tesis, algunos aspectos cobraron importancia, y se explicarán para tener en cuenta en futuros trabajos.

2. Teoría utilizada:

Las siguientes correlaciones se utilizan para predecir la región de transición sobre una placa plana [4]:

$$Nu_{trans} = Nu_{lam}(Re_l, \mathrm{Pr}) \left(\frac{Re_x}{Re_l}\right)^c \quad (1)$$

$$Re_l = 3.6\ 10^5 \left(\frac{100\ u_r'}{u_\infty}\right)^{-\frac{5}{4}} \tag{2}$$

$$c = 0.9922\ log_{10}\ Re_l - 3.013 \tag{3}$$

$$Nu_{turb} = 0.0296\ Re_x^{0.8}\ Pr^{0.6} \tag{4}$$

$$Nu_x = \left[Nu_{lam}^5 + (Nu_{trans}^{-10} + Nu_{turb}^{-10})^{-\frac{1}{2}}\right]^{\frac{1}{5}} \tag{5}$$

Como las propiedades del fluido van a variar significativamente, es importante hacer algunas correcciones. Las correlaciones para flujo externo deben evaluarse a la temperatura de la corriente libre (T_∞) y el resultado debe multiplicarse por la relación de temperatura absoluta $(T_w / T_\infty)^{-n}$, con n en el rango de 0,25 a 0,4. [4].

El método de resistencia térmica es una forma de resolver problemas sencillos de 1D [5]:

$$q_x = \frac{T_{\infty,1} - T_{\infty,2}}{R_{total}} \tag{6}$$

Para el modelo de turbulencia, se utiliza Shear Stress Transport [6] y el modelo Gamma Theta [7] para la región laminar y de transición.

3. Verificación de placa plana:

La geometría más simple se utiliza para validar ambos métodos. La placa plana se ejecuta con las condiciones de contorno del STRUT, como la intensidad de la turbulencia o la temperatura de la pared.

La simulación con régimen totalmente turbulento sobre la placa plana tiene un coeficiente de transferencia de calor medio de $709.551\ W/m^2\ K$, lo mismo para las correlaciones con diferentes factores n con resultados $676.349\ W/m^2\ K$ para $n = -0.25$, $726.261\ W/m^2\ K$ para $n = -0.3$, y $779.911\ W/m^2\ K$ para $n = -0.35$.

La simulación con el modelo de transición sobre la placa plana tiene un coeficiente de transferencia de calor medio de $655.227\ W/m^2\ K$, lo mismo para las correlaciones con diferentes factores n con resultados $675.01\ W/m^2\ K$ para $n = -0.25$, $704.64\ W/m^2\ K$ para $n = -0.3$, y $757.62\ W/m^2\ K$ para $n = -0.35$.

El modelo totalmente turbulento predice bien en general la transferencia de calor, pero con una diferencia del 3% en el coeficiente de transferencia de calor promedio para el factor n = -0,3, que en cada simulación parece que es el valor correcto para estas mediciones. Sin embargo, las correlaciones predicen en exceso el número de Reynolds de inicio, que es solo función de la intensidad de la turbulencia de entrada. Además, la placa plana predice una enorme transición repentina donde esta región es prácticamente nula, mientras que las correlaciones dan como resultado una transición abrupta pero no tan rápida como la placa plana.

4. Simulacioness:

Hay pasos muy importantes y marcados para ejecutar una simulación.

1.- Geometría: Es proporcionada por el Departamento de Chalmers.

2.- Malla: Es importante tener un valor a medio término de buena malla y tiempo de simulación porque las simulaciones más pesadas pueden tardar cerca de 24 horas en converger. Una variable muy importante en CFD es el Y Plus porque mide la distancia entre la pared y la primera capa de celdas. Para estos modelos se necesita a y + <1 para capturar correctamente la capa viscosa, para lograrlo se necesita una malla de refinamiento cerca de la pared.

3.- Montaje: Donde se seleccionan las condiciones de contorno, fluido y modelo de turbulencia. Algunos límites los proporciona el Departamento de Chalmers, el fluido es Aire Gas Ideal con propiedades variables con la temperatura, este varía demasiado y puede conducir a una diferencia cercana al 20% del coeficiente de transferencia de calor. Se realiza un problema básico de transferencia de calor para estimar la temperatura de la pared del STRUT que tiene aire fluyendo a 377K e Hidrógeno fluyendo dentro de la paleta a 25ºK.

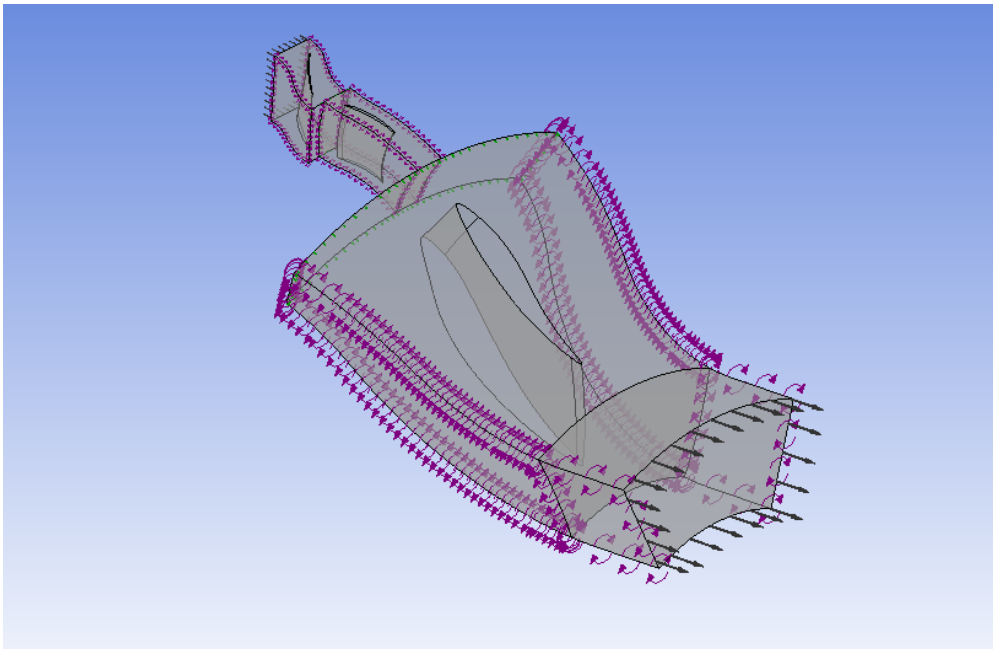

Ilustración 1: Modelo de simulación

5. Resultados y conclusión:

Para el modelo completamente turbulento, se realiza un estudio de independencia de la malla para lograr el valor más realista, 734 W⁄ (m ^ 2 K). Se realiza una comparación entre tener propiedades constantes y variables, con un resultado de un aumento del 19,89% del coeficiente de transferencia de calor. Otra comparación se realiza simulando la configuración principal con diferentes temperaturas de pared. Hasta un límite, la disminución de la temperatura de la pared conduce a una menor transferencia de calor.

En conclusión, el modelo completamente turbulento predice bastante bien los fenómenos si el exponente n deseado es -0,35 que se encuentra en el rango proporcionado. Se muestran otros factores que exaltan la relevancia del mismo, como la enorme variación de la transferencia de calor sin tener en cuenta las propiedades variables o la diferente temperatura de la pared.

En contraste con el modelo completamente turbulento, el modelo de transición difiere significativamente de las correlaciones incluso en la placa plana. Los cambios más significativos son el número de Reynolds de inicio, que marca cuándo ocurre la transición y, por lo tanto, es una gran diferencia porque las correlaciones para la intensidad turbulenta de entrada predicen una región laminar mínima. También hay que tener en cuenta que se ha escogido el grado de turbulencia al inicio del ICD y no justo en el inicio del STRUT, por lo que puede haber una disminución de la intensidad que genere una transición posterior y que se adecúe más a las simulaciones. Incluso en ambas simulaciones hay una enorme diferencia de coeficiente de transferencia de calor en la región turbulenta, donde debería superponerse prácticamente como en el modelo totalmente turbulento; obviamente, esta variación da como resultado una compensación en el coeficiente de transferencia de calor promedio.

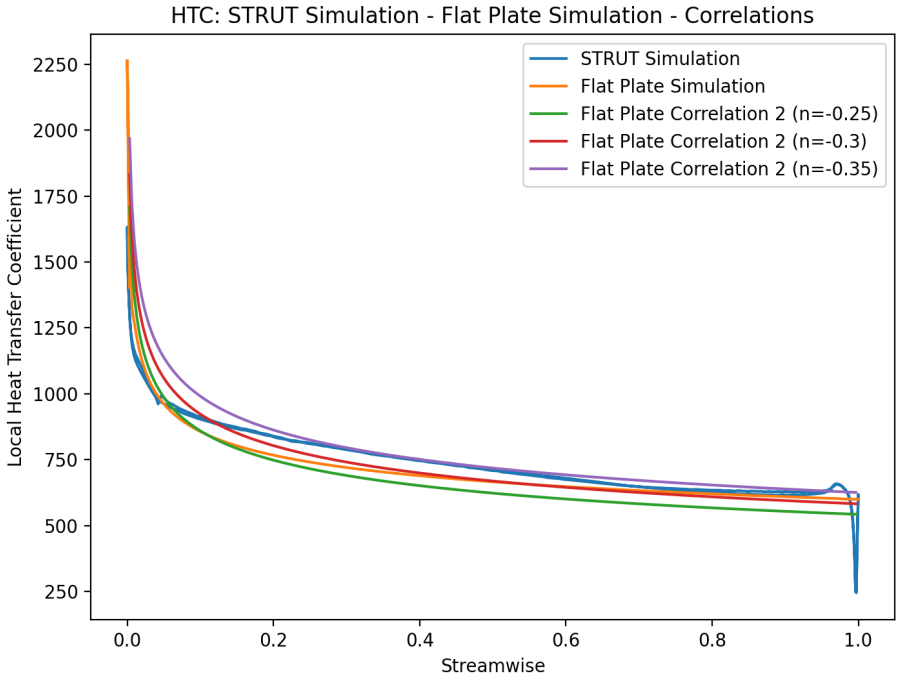

Ilustración 2: Coeficiente de transferencia de calor local para las correlaciones, la verificación de placa plana y la simulación para el modelo totalmente turbulento.

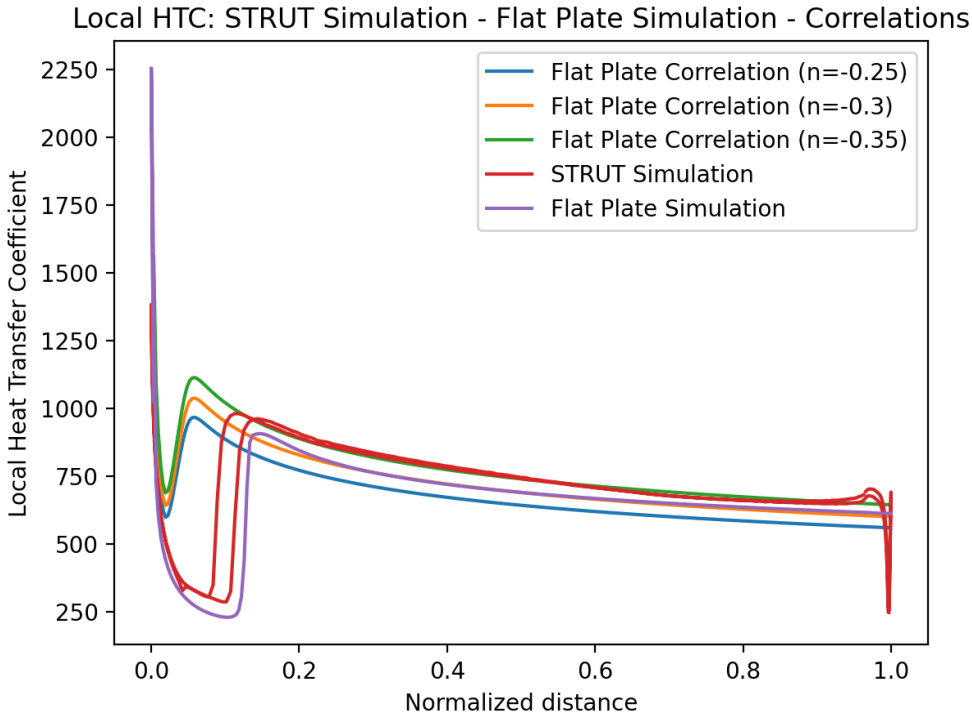

Ilustración 3:Coeficiente de transferencia de calor local para las correlaciones, la verificación de placa plana y la simulación para el modelo de transición.

6. Bibliografía:

[1] Ansys CFX: Turbomachinery CFD Software: https://www.ansys.com/products/fluids/ansys-cfx

[2] MathWorks MATLAB: https://es.mathworks.com/products/matlab.html

[3] Python: https://www.python.org/

[4] John H. Lienhard V, "Heat Transfer in Flat-Plate Boundary Layers: A correlation for Laminar, Transitional, and Turbulent Flow", June 2020.

[5] Theodore L Bergman, Adrienne S. Lavine, Frank P. Incropera, David P. Dewitt, "FUNDAMENTALS OF HEAT and MASS TRANSFER", Seventh Edition.

[6] Menter, F.R., "Two-Equation Eddy-Viscosity Turbulence Models for Engineering Applications", August 1994.

[7] R.B. Langtry, "A Correlation-Based Transition Model using Local Variables for Unstructured Parallelized CFD Code", 2006.

CONCEPTUAL DESIGN OF COMPACT HEAT EXCHANGER TECHNOLOGY FOR HYDROGEN FUELED AIRCRAFT

Author: Ureña Álvarez, Pedro.
Supervisor: Xisto, Carlos.
Collaborating Entity: ICAI – Universidad Pontificia Comillas.

ABSTRACT

This project is a heat transfer study over a structural vane in a ICD (Interconecting Duct). The workflow is to previously have a background of CFD (Computational Fluid Mechanics), have an overlook into turbulence models, validate the turbulence model via flat plate verification, and simulate the main network.

Keywords: CFD, Heat Transfer, Air, Hydrogen, ANSYS, CFX.

7. Introduction:

This project takes place as a consequence of trying to predict the Heat Transfer Coefficient in the STRUT; and also to get closer in understanding the fluid systems in heat exchangers when the temperature difference is significant between the freestream and the wall temperature, about all when working in low temperature conditions (<100K). HTC will be calculated running simulations in the 3D model and a Flat Plate Verification in Ansys CFX 2021 R1 [1]; also, it will be compared with numerical correlations with help of MATLAB R2019b [2] and Python 3 [3] with other libraires. During the thesis, some aspects became important, and they will be explained to take in account in future work.

8. Theory used:

The following correlations are used for predicting the transition region over a flat plate [4].

$$Nu_{trans} = Nu_{lam}(Re_l, \mathrm{Pr}) \left(\frac{Re_x}{Re_l}\right)^c \tag{1}$$

$$Re_l = 3.6\ 10^5 \left(\frac{100\ u_r'}{u_\infty}\right)^{-\frac{5}{4}} \tag{2}$$

$$c = 0.9922\ log_{10}\ Re_l - 3.013 \tag{3}$$

$$Nu_{turb} = 0.0296\ Re_x^{0.8}\ Pr^{0.6} \tag{4}$$

$$Nu_x = \left[Nu_{lam}^5 + (Nu_{trans}^{-10} + Nu_{turb}^{-10})^{-\frac{1}{2}}\right]^{\frac{1}{5}} \tag{5}$$

As the properties of the fluid is going to vary significantly, it is important to make some corrections. The correlations must be evaluated at the freestream temperature (T_∞) and result multiplied by the absolute temperature ratio $(T_w/\ T_\infty)^{-n}$, with n in the range of 0.25 to 0.4. [4].

The thermal resistance method is a way of solving easy 1D problems [5].

$$q_x = \frac{T_{\infty,1} - T_{\infty,2}}{R_{total}} \tag{37}$$

For the turbulence model, Shear Stress Transport [6] is used, and the Gamma Theta Model [7] for the laminar and transition region.

9. Flat plate validation:

The simplest geometry is used to validate both methods. The flat plate is run with the boundary conditions of the STRUT, such as turbulence intensity or wall temperature.

The fully turbulent flat plate simulation finalizes with an average heat transfer coefficient of $709.551\ W/m^2\ K$, same for the correlations for different n factor results on $676.349\ W/m^2\ K$ for $n = -0.25$, $726.261\ W/m^2\ K$ for $n = -0.3$, and $779.911\ W/m^2\ K$ for $n = -0.35$.

The transition flat plate case leads an average heat transfer coefficient of $655.227\ W/m^2\ K$, and correlations for different n factor results on $675.01\ W/m^2\ K$ for $n = -0.25$, $704.64\ W/m^2\ K$ for $n = -0.3$, and $757.62\ W/m^2\ K$ for $n = -0.35$.

The fully turbulent model predicts overall well the heat transfer but with a difference of 3% in the average heat transfer coefficient for the $n = -0.3$ factor, that in each simulation seems that is the correct value for these measurements. Nevertheless, the correlations overpredicts the onset Reynolds number, that is only function of the inlet turbulence intensity. Furthermore, the flat plate predicts a huge sudden transition where

this region is practically neglected, while the correlations result on an abrupt transition but not as snappish as the flat plate.

10. Simulations:

There are very important and marked steps to run a simulation.

1.- Geometry: Is provided by the Chalmers Department.

2.- Mesh: It is important to have a midterm value of good mesh and simulation time because the heaviest simulations can take near 24 hours to converge. A very important variable on CFD is the Y Plus because it measures the distance between the wall and the first cell layer. For these models it is needed a $y^+ < 1$ to correctly capture the viscous layer, to achieve it is needed a near-wall refinement mesh.

3.- Setup: Where the boundaries, fluid and turbulence model are selected. Some boundaries are provided by the Chalmers Department, fluid is Air Ideal Gas with variable properties with the temperature, this this one varies too much and can lead on a difference of near 20% of heat transfer coefficient. A basic heat transfer problem is done to estimate the wall temperature of the STRUT having air flowing at 377K and Hydrogen flowing inside the vane at 25ºK.

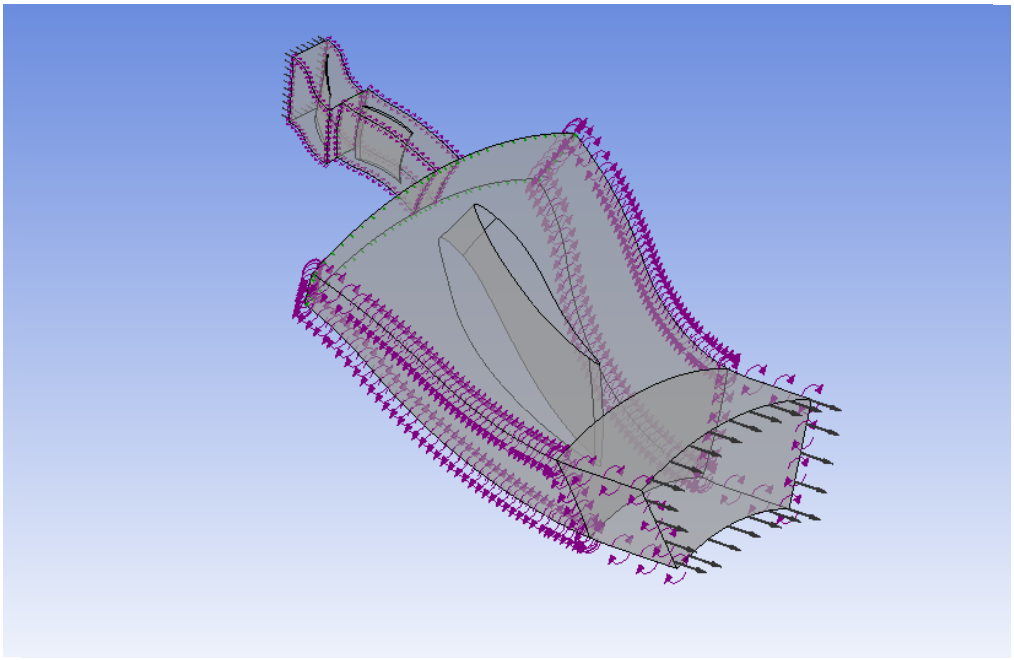

Figure 1: Simulation network.

11. Results and conclusion:

There are very important and marked steps to run a simulation. For the fully turbulent model, a mesh independence study is done to achieve the most realistic value, $734\ W/m^2\ K$. A comparison between having constant and variable properties is done, with a result of an increase of 19.89 % of heat transfer coefficient. Another comparison

is done by simulating the main configuration with different wall temperatures. Up to a limit, decreasing the wall temperature leads on having less heat transfer.

In conclusion, the fully turbulent model predicts quite well the phenomena if the desired n exponent is -0.35 that is in the provided range. Other factors are shown to exalt the relevance of it, such as the huge variation of the heat transfer without taken in account the variable properties or the different wall temperature.

In contrast with the fully turbulent model, the transition model differs significantly from the correlations even in the flat plate. The most significant changes are the onset Reynolds number, that marks when the transition occurs and thereby is a huge difference because the correlations for the inlet turbulent intensity predicts a minimum laminar region, and the length of the transition region, that the simulations predict a very vanish region. It is important to highlight that the turbulence intensity used is the one at the ICD inlet, not at the STRUT start, so there may be a decay between these two points that leads on a lower turbulence intensity and thereby an approximation between the simulations and the correlations. Even in both simulations there is a huge difference of heat transfer coefficient in the turbulent region, where should be practically superimposed as in the fully turbulent model; obviously this offset results in a offset in the average heat transfer coefficient.

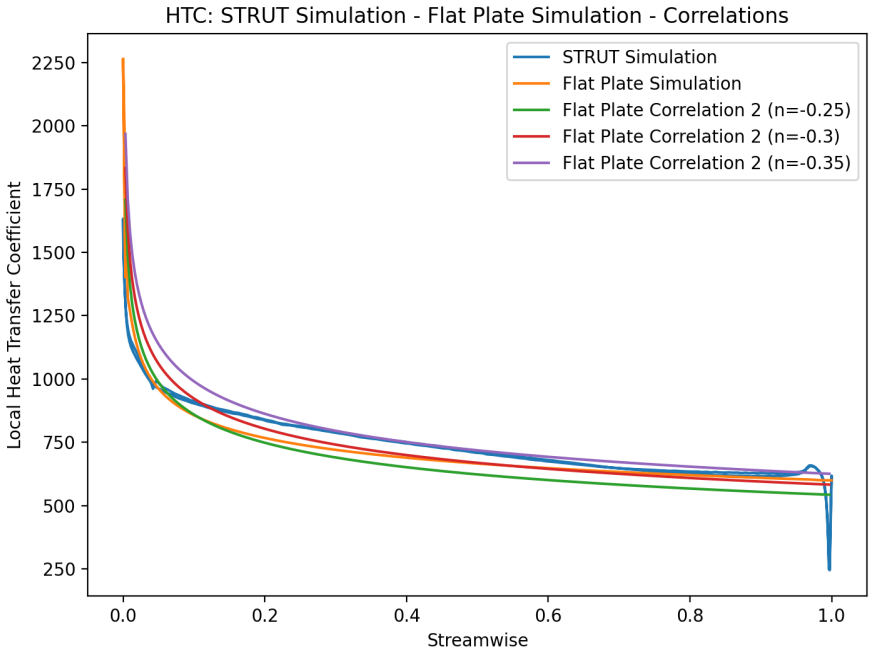

Figure 2: Comparison in the fully turbulent model of the heat transfer coefficient from the whole package simulation, flat plate simulation and correlations.

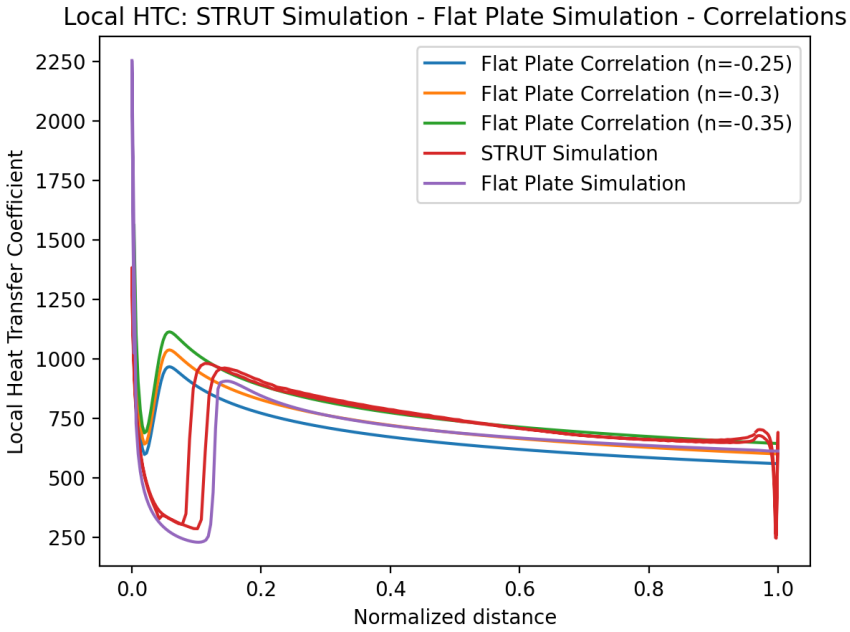

Figure 3:Comparison of the transition model of the heat transfer coefficient from the whole package simulation, flat plate simulation and correlations.

12. Bibliografía:

[1] Ansys CFX: Turbomachinery CFD Software: https://www.ansys.com/products/fluids/ansys-cfx

[2] MathWorks MATLAB: https://es.mathworks.com/products/matlab.html

[3] Python: https://www.python.org/

[4] John H. Lienhard V, "Heat Transfer in Flat-Plate Boundary Layers: A correlation for Laminar, Transitional, and Turbulent Flow", June 2020.

[5] Theodore L Bergman, Adrienne S. Lavine, Frank P. Incropera, David P. Dewitt, "FUNDAMENTALS OF HEAT and MASS TRANSFER", Seventh Edition.

[6] Menter, F.R., "Two-Equation Eddy-Viscosity Turbulence Models for Engineering Applications", August 1994.

[7] R.B. Langtry, "A Correlation-Based Transition Model using Local Variables for Unstructured Parallelized CFD Code", 2006.

Contents

Table Index

Figure Index

CHAPTER 1: ABSTRACT

ENABLEH2 [1] is a project among several European Universities and organizations with the aim of lending a hand to reduce 75% of the CO2 (carbon dioxide) emissions and 90% of the NOx (nitrogen oxides) by 2050, helping the European Green Deal [2]. This project exalts the great role that liquid hydrogen (LH2) can have in the incoming hydrogen powered aviation technology.

The main scope of this project is to study the heat transfer in the Interconnecting Compressor Duct (ICD), in particular the Structure Vane (STRUT), of the previously and currently studied low-pressure compressor from "FEASIBILITY OF A RADICAL VANE-INTEGRATED HEAT EXCHANGER FOR TURBOFAN ENGINE APPLICATIONS" [3]. In the previous study, different design configurations were discussed for the duct and this project will be run in the Configuration 1. The principal issue will be shed light on heat transfer behavior having LH2 flowing inside the STRUT so the temperature difference between the freestream and the wall is high, so how it is improved.

To carry it out, simulations will be made using CFD for the given conditions and the importance of some aspects at the time of running will also be written about. These simulations will be contrasted with flat plate verification on CFD. The results will also be compared with theoretical correlations and data from previous studies, although it is hoped that in the future data will be obtained from a real case.

CHAPTER 2: INTRODUCTION

The cooling technique over the compressor vanes to extract heat can generate a decrease in the total pressure loss between 5.9% and 12%, increase in thermal efficiency and therefore better efficiency [4]. This advance in performance can let on having less weight or more aggressive designs, which leads on having an axial shorter compressor with a higher radial difference (S duct).

This project takes place as a consequence of trying to predict the Heat Transfer Coefficient in the STRUT of the previous work; and also to get closer in understanding the fluid systems in heat exchangers when the temperature difference is significant between the freestream and the wall temperature, about all when working at high temperature differences. HTC will be calculated running simulations in the 3D model and a Flat Plate Verification in Ansys CFX 2021 R1 [5]; also, it will be compared with numerical correlations with help of MATLAB R2019b [6] and Python 3 [7] with other libraries then explained. During the thesis, some aspects became important, and they will be explained to take in account in future work.

The arrangement of the compact heat exchanger is a three-stage low-pressure compressor (LPC), an Outlet Guide Vane (OGV) Heat Exchanger (HEX), Interconnecting Compressor Duct (ICD) HEX where the Structure Vane (STRUT) is, Inlet Guide Vane (IGV) HEX, and the High Pressure Compressor (HPC). The OGV will direct the flow downwards because, to make it shorter, it has an S form. The STRUT is a supporting structure whose main purpose is to carry the load from the bearing to the engine mount. “In a multi-spool gas turbine, annular interconnecting ducts (ICD) are used to connect the low/intermediate-pressure compressor to the high-pressure compressor. The duct is commonly referred as S-ducts due to the radial offset required by the different compressor spools. From an aero-perspective the ICD should be designed to transfer the flow radially with minimal losses and to provide a uniform temperature and pressure distribution at the

HPC inlet." [3] A scheme of the whole HEX is presented on Figure 1. The 3D model where the simulations were run with the R3, OGV and S-DUCT can be watched in Figure 2.

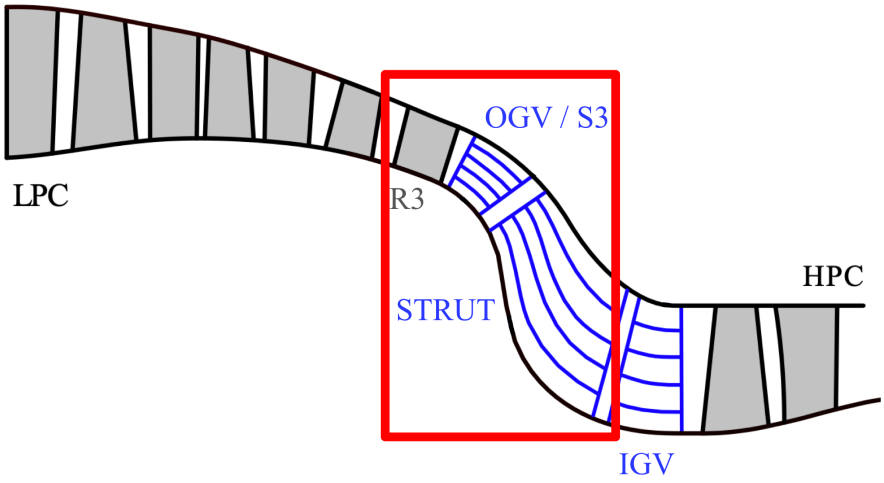

Figure 1: Scheme of the whole HEX network

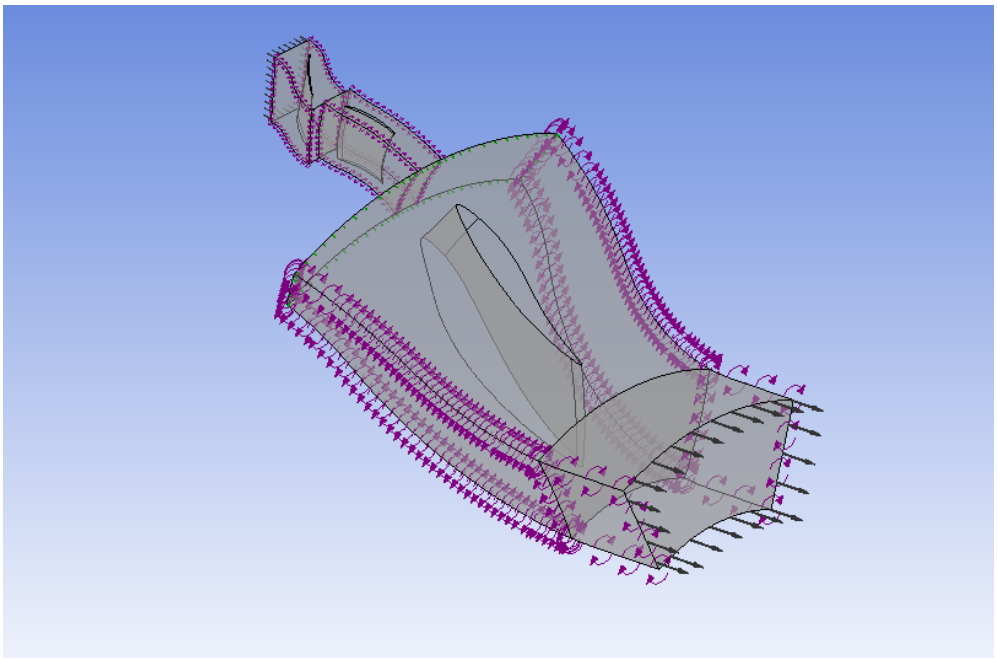

Figure 2: S3, R3 and ICD geometry.

As some of the characteristics are not fixed at the moment of this report, assumptions and starting points will be presented when it is necessary.

First, some research needs to be done to perform correctly and be able to discuss results, some of these previous investigations will have an insight afterwards such as correlations for the numerical approach, turbulent models or the effect of temperature and pressure on the variable properties and subsequently on the results.

Second, refine the 3D fully turbulent model mesh to achieve good accuracy. Make an assumption on how the LH_2 flows in the blade and thereby compute a code to have a starting constant wall temperature of the STRUT. The simulations much carry out a mesh independence study. At the same time, some simulations are run for different wall temperature and the impact of this can be discussed.

Then, simulations with the same boundary conditions are done for a Flat Plate.

Next, it is computed a code to compare the previous results with the numerical correlations.

Finally, it is done a small insight with the transition model.

CHAPTER 3: SUSTAINABLE DEVELOPMENT GOALS (SDG)

The United Nations has taken an initiative to improve the planet in a general way, not only for humans, in all areas but also for the planet encompassing animals, ecosystems and the future. All the countries that make up the United Nations should, as far as possible, adopt measures to achieve this. The measures must be in line with the rest of the objectives in such a way that improving social status must take into account that it should improve or not worsen the conditions of the ecosystems.

There are 17 Goals in total, which are: No poverty, Zero hunger, Good health and well-being, Quality education, Gender equality, Clean water and sanitation, Affordable and clean energy, Decent work and economic growth, Industry, innovation and infrastructure, Reduced inequalities, Sustainable cities and communities, Responsible consumption and production, Climate action, Life below water, Life on land, Peace, justice and strong institutions, and Partnerships for the goals. The main objective of the overall project is related with the 13th goal, Climate action, and the way to improve it is by working in the 9th goal, Industry, innovation and infrastructure. Climate change is affecting all countries on all continents. It is disrupting national economies and affecting different lives. Weather systems are changing, sea levels are rising, and weather events are becoming increasingly extreme. In recent years, temperatures have not stopped rising since each year that passes is also the hottest to date and it is necessary to take measures because they were not going to achieve one 1.5 or 2 ° C of the Paris goal. Companies and governments are key to this objective because a transition must be made so that everything around us is good for the environment. This project will try to make nearer the challenge of reducing 75% of the CO2 emissions from aviation. Without improvements in innovation, the rest of the objectives are quite limited since thanks to technology many of them can be improved. An improvement in urban or rural transport for civilians can have an improvement in health if they produce less

dangerous gases for human beings, also if it is better for the environment because it does not produce harmful gases. The improvement in transport can also improve different points such as hunger, poverty, education, health, equality, water or work because it can make available resources that before and did not have. Another secondary goals are Good health and well-being (3), Life on land (15) and Affordable and clean energy (7). With improvement in transport sector, nocive gases will be reduced in pro of humans, animals and the whole Earth ecosystem. This could be the first step of the conversion of the aviation into a cleaner way.

CHAPTER 4: THEORETICAL BACKGROUND

1 INTRODUCTION:

In order to a better understanding of this work, a short introduction on basic knowledge of heat transfer and fluid dynamics will be necessary. A small brushstroke will be given on the most basic knowledge but also on more advanced knowledge, which is very important to understand this document and the procedure.

2 BASIC HEAT TRANSFER:

Heat transfer is thermal energy in transit due to a temperature difference through a medium. Without the condition of temperature difference, there will not be heat transfer.

There are 3 main ways of heat transfer: Conduction, Convection and Radiation, and they can be mixed up.

When a temperature gradient occurs in a medium, like solid or fluid, we refer to the heat transfer that will take place across the medium as conduction.

Convection, on the other hand, refers to heat transfer between a surface and a moving fluid when their temperatures are different.

Thermal radiation is the third way of heat transport because all surfaces of finite temperatures emit energy in the form of electromagnetic waves. Radiation is a phenomena that is negligible compared with convection in this case due to the relatively low temperatures and the idea is to have a first insight so will no longer be studied. [8]

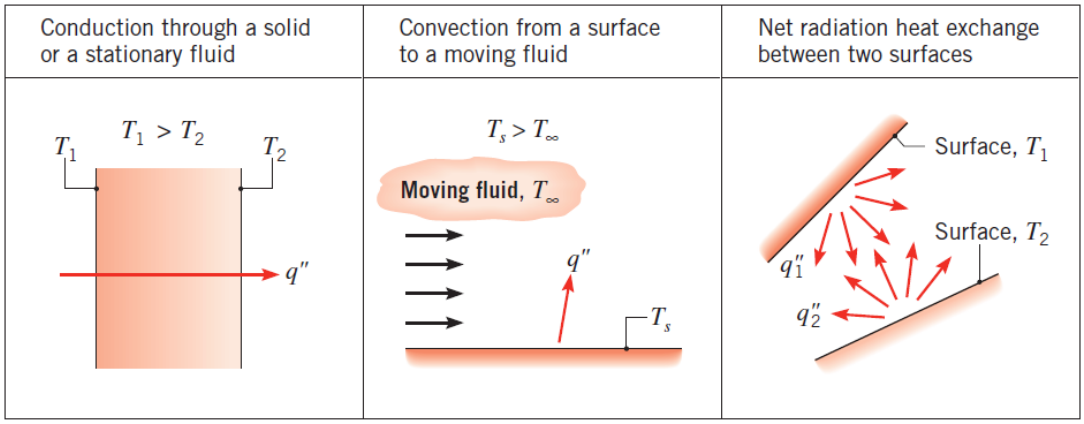

Figure 3: Heat transfer ways sketch [8]

2.1 CONDUCTION:

Conduction is made by the transfer of energy from the most energetic particles (more temperature leads to higher energy) to the less energetic particles in the same medium due to interaction between them such as collisions.

Hopefully, conduction is well-known at the state of the art at it is easily predicable by the general Fouriers Law:

$$\boldsymbol{q}'' = -k\boldsymbol{\nabla}T = -k\left(\boldsymbol{i}\frac{\partial T}{\partial x} + \boldsymbol{j}\frac{\partial T}{\partial y} + \boldsymbol{k}\frac{\partial T}{\partial z}\right) \tag{1}$$

This general law can be easily simplified if it is just studied the heat transfer in one direction, making the vector equation into a scalar equation:

$$q_x'' = -k\frac{dT}{dx} \tag{2}$$

The heat flux q_x'' is the amount of heat per unit area perpendicular to the axis, so the units are W/m^2.

The thermal conductivity k is a property of each material that reflects how well does it transfer the heat. This will be discussed on Section X donde hablo de la k con T.

The temperature gradient $\frac{dT}{dx}$ denotes how temperature varies along the distance. It is needed a negative sign (–) because the heat transfer goes in the direction of decreasing temperature, which is the opposite of the gradient.

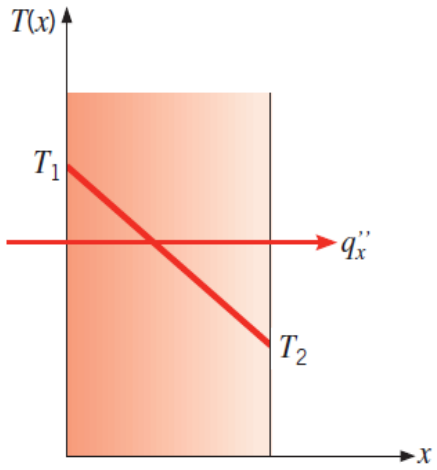

Figure 4: Heat direction and temperature [8]

2.1.1 THERMAL CONDUCTIVITY:

A material with high k will lead into high heat flux so, at the first insight, should be easy to think that a better k is always the best idea to increase the heat transfer coefficient. This property also changes with temperature and in some cases, there is huge difference.

It depends on the conditions of the microscopic energy carriers of the material: thermal mass (c), velocity ($\bar{v}$) and the number density (n); and in the relationship among them: distance between collision (L). Thermal conductivity is a product of the previous variables as seen in Equation 3.

$$k = nc\bar{v}L \tag{3}$$

Thermal conductivity is a function of the temperature and pressure conditions, but for most of solids, liquids, and low-pressure ideal gases, is practically independent of pressure [9]. Thereby, for the solid study it will be just focus on the temperature dependence.

The main energy transfer character in gases is the transfer of kinetic energy throw collisions between the high-energy-temperature-velocity particles and the low-energy-temperature-velocity particles. Thus, having lower temperature will deal on having less particles velocity as it is related with the temperature and the transference of energy is lower. The dependence can be calculated analogically as by Sutherland's formula [10]

$$\frac{k}{k_0} = \left(\frac{T}{T_0}\right)^c \left(\frac{T_0 + S_k}{T + S_k}\right) \tag{4}$$

	T_0	k_0	S_k	c
Air	273 K	$0.0241\ {}^{W}/_{m}$	194 K	1.5

Table 1:Air's Sutherland's formula coefficients.

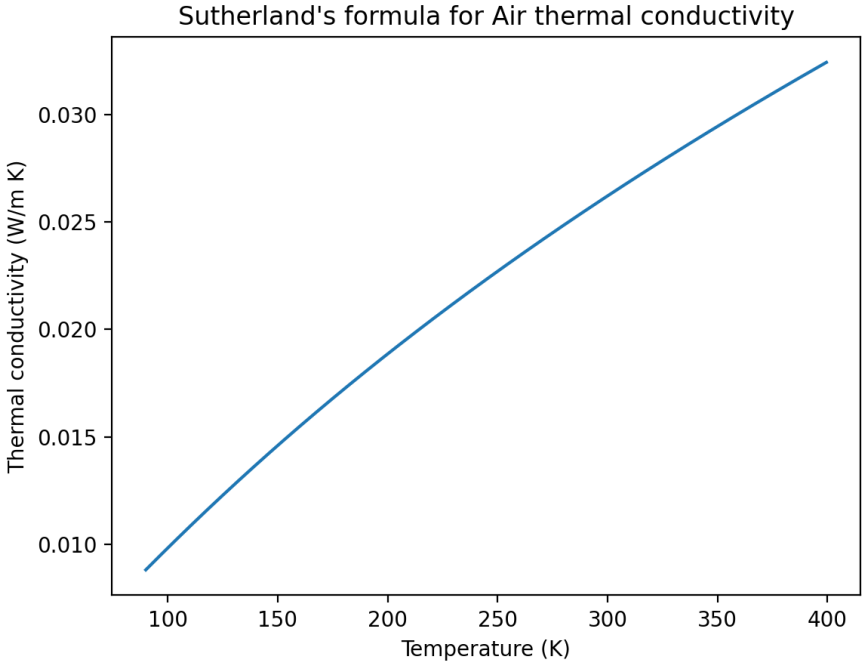

Figure 5: Air Thermal conductivity as a function of temperature by Sutherland's formula

In liquids, as the density is in most of the times higher, the distance between the molecules is lower. Previously, it is said that in gases the energy is transferred primarily by kinetic energy transfer in collisions, but in liquids the main way of energy transport is vibrational due to intermolecular forces between the molecules.

The transfer method in solids is thermal vibration and approached by particles called phonons that travel at the speed of sound (velocity at which waves propagate through a material) in the material, which is referenced as phonon conduction.

For metal good electrical conductors, the transport is a sum of the phonon energy transfer (k_{ph}) and electron energy transport (k_{el}).

$$k = k_{ph} + k_{el} \tag{5}$$

At room temperatures and higher, the electron transport factor is the main.

At cryogenic temperatures, there are two additional effects on electron energy transport, phonons' interferences ($k_{el,ph}$) and lattice imperfection's interferences ($k_{el,im}$) due to dislocations or impurities.

$$\frac{1}{k_{el}} = \frac{1}{k_{el,ph}} + \frac{1}{k_{el,im}} \tag{6}$$

Referring to Equation 3, the number of impurities is not dependent of temperature, density and velocity are practically constant, and specific heat is directly proportional to the absolute temperature. Thermal conductivity of phonons' interferences is inversely proportional to the square of temperature. Combining both factors, at very low temperatures the T^3 component is insignificant, so k_{el} is proportional to T; at some temperature the T^3 component becomes significant and k_{el} is inversely proportional to T^2. At extremely low temperatures, such as 50 K, the thermal conductivity can rise 37% compared at room temperatures as shown in Figure 10.

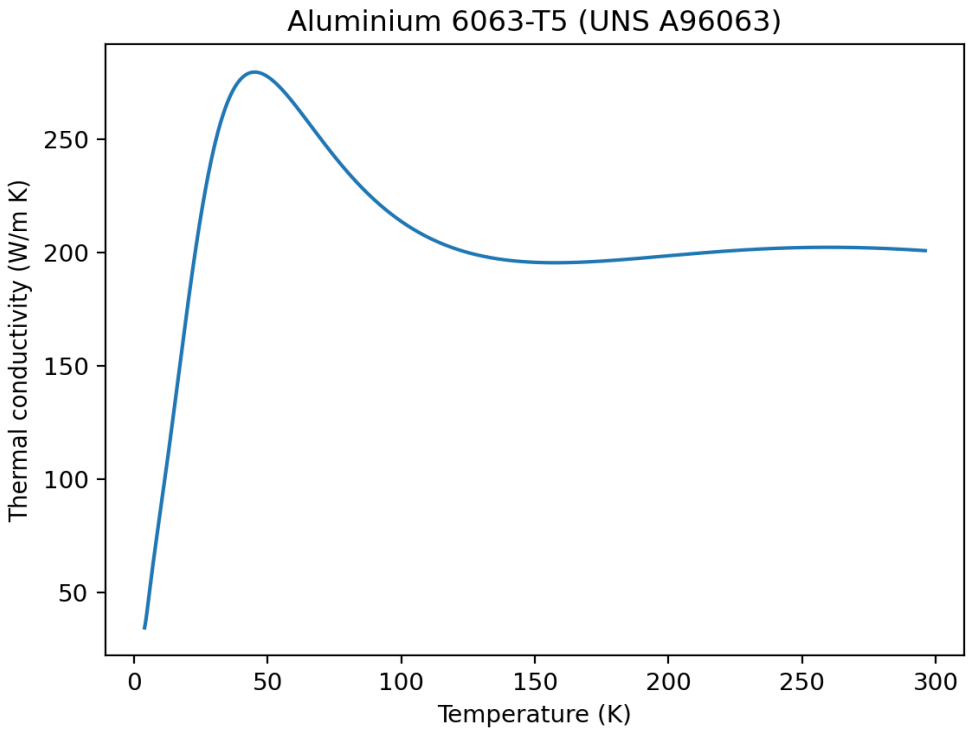

Figure 6: Aluminum Thermal Conductivity dependency with temperature

2.2 CONVECTION:

In convection, the energy is transferred by diffusion (random molecular motion) and advection (macroscopic motion of the fluid). The diffusion factor is the main in near the surface due to its low velocity, even the only mechanism when it reaches the surface ($y = 0$) and velocity is zero.

There are two main types, forced and natural, and their mixture. Natural is related with density differences due to temperature variation, the so-called buoyancy forces. Forced is caused by external forces such as a fan or pump.

The convection heat transfer is modelled by the Newtons law of cooling:

$$q'' = h\,(T_s - T_\infty) \tag{7}$$

Where T_s is the surface temperature and T_∞ the freestream fluid temperature. The h ($W/m^2\,K$) parameter is called convection heat transfer coefficient and depends on mostly overall conditions in the boundary layer like geometry, nature of the fluid motion, thermodynamic and transport properties.

2.2.1 VELOCITY BOUNDARY LAYER:

When a fluid flows over a surface there is a velocity boundary layer, this is the part of the fluid flow that becomes slower due to the contact of the surface. When a particle touches the surface, the velocity becomes zero due to the viscosity; and each particle retard the beside particle until there are no disturbance and has the freestream velocity (u_∞). This retardation of fluid motion is due to shear stresses (τ) acting in planes parallel to the fluid velocity. The boundary layer thickness (δ) is the y value for which $u = 0.99\,u_\infty$.

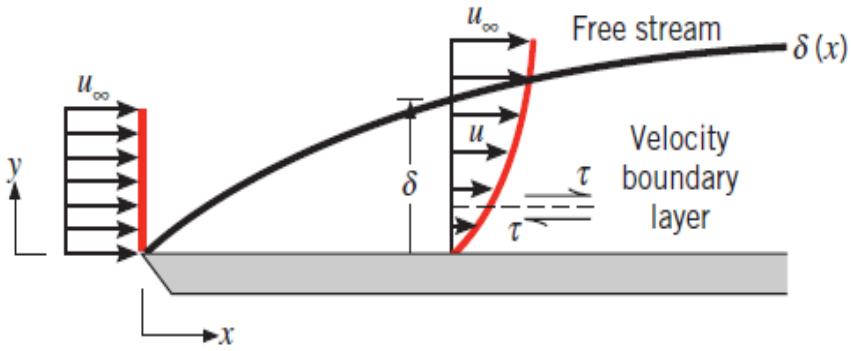

Figure 7: Velocity boundary layer developing over a flat plate. [8]

Furthermore, there are different regions that can be distinguish in the boundary layer. These are the laminar, transition and turbulent regions. The laminar region uses to be highly ordered until it reaches the transition regions where it is found a conversion between laminar and turbulent characteristics. The turbulent region is marked by highly irregular and random flow motion, its mixing is dependent on the appearance of vortices (streaks). In the turbulence part can also be perceive a viscous sublayer with nearly laminar properties, an adjoining buffer layer in which diffusion and turbulent mixing are on a par, and a turbulent zone where mixing is the dominant.

The transition part is one of the toughest parts to approach and its onset is highly dependent on a dimensionless parameter called Reynolds number (Re). It is the ratio between inertia and viscous forces, so when viscous forces are high there is laminar region and the opposite for turbulent region. On a flat plate, the critical Reynolds number (Re_c), where the transition begins, is between 10^5 and $3 * 10^6$ depending on surface roughness and the turbulence intensity of the freestream, but a well-used $Re_{x,c}$ is $5 * 10^5$. ρ is the fluid density, μ is the fluid dynamic viscosity and x is the distance from the leading edge.

$$Re_x = \frac{\rho u_\infty x}{\mu} \tag{8}$$

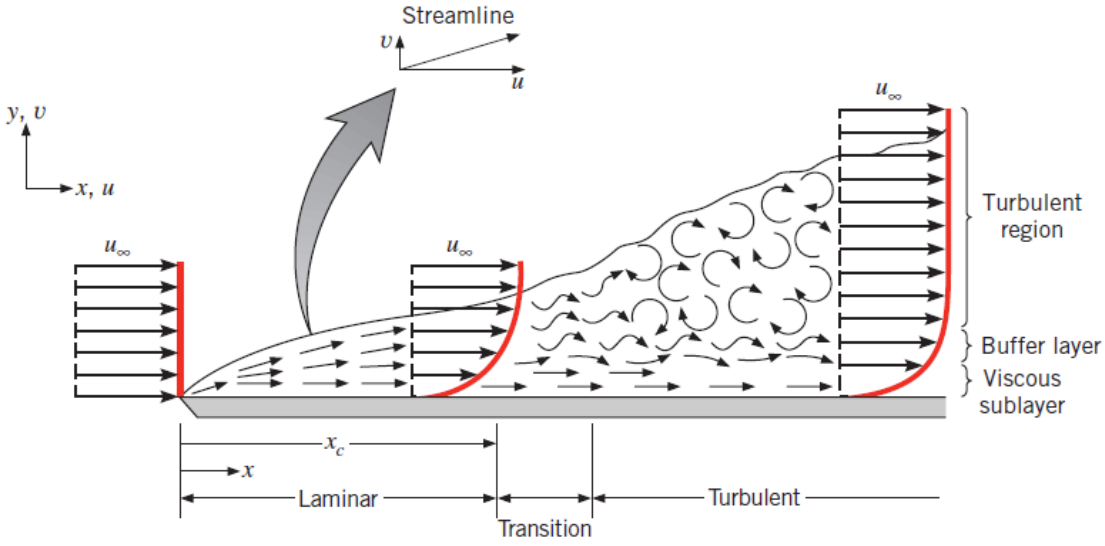

Figure 8: Velocity boundary layer development on a flat plate [8]

2.2.2 THERMAL BOUNDARY LAYER:

With the introduction of the velocity boundary layer as an effect of velocity difference, it is consequently the appearance the thermal boundary layer as an effect of temperature difference between the fluid and the wall. Particles exchange heat with those among them, from the hottest to the coldest, which creates a temperature gradient and thereby a thermal boundary layer thickness (δ_t) for which $\frac{T_s - T}{T_s - T_\infty} = 0.99$.

In the transition region there is a huge variation of the heat transfer coefficient and in the turbulent region it is bigger due to the continuous exchange in mass and heat between layers and more agitation.

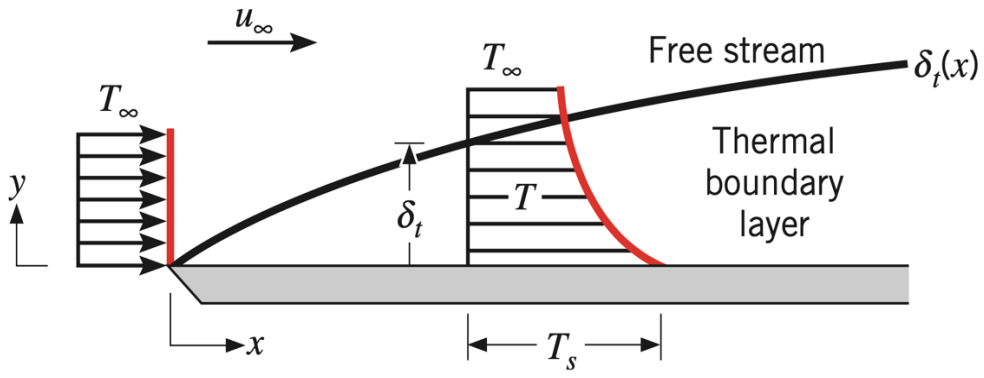

Figure 9: Thermal boundary layer over a flat plate with more temperature than the freestream's [8]

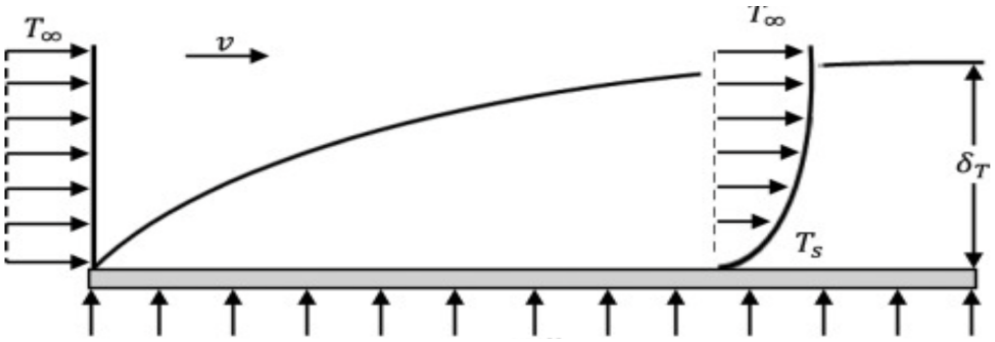

Figure 11:Thermal boundary layer over a flat plate with less temperature than the freestream's [8]

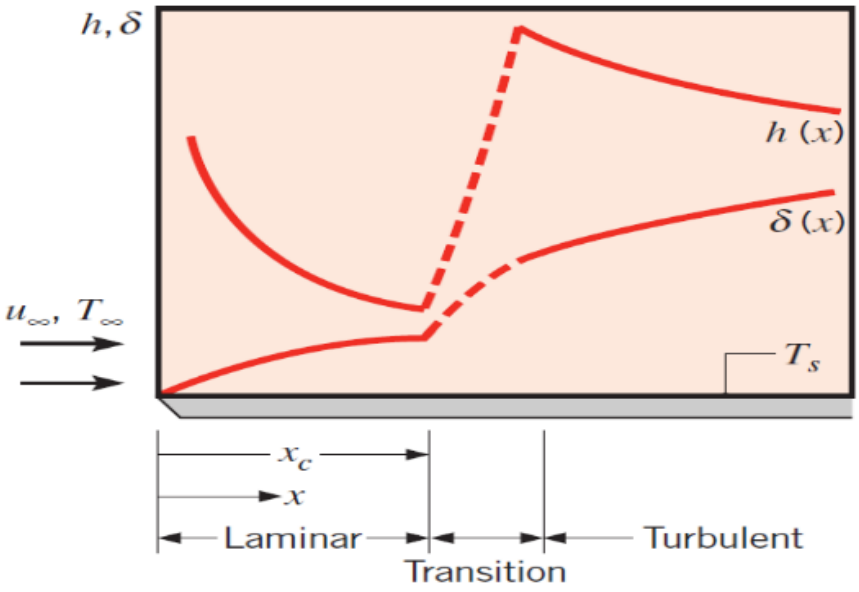

Figure 10: Heat transfer coefficient variation with boundary layer. [8]

2.3 DIMENSIONLESS NUMBERS:

This numbers are pure and have no physical units (coming up by a sort of operations like multiplication or division) but have an important physical meaning. The study of this numbers can lead on understanding the fluid's behavior or extrapolate a problem to a bigger or smaller one.

2.3.1 REYNOLDS NUMBER:

Relates the viscous forces with the inertial forces. Re describes the fluid flow pattern; if the viscous forces are larger than the inertial forces, the flow will be laminar (ordered), and if the inertia forces are bigger than the viscous forces, then flow will be turbulent (chaotic).

$$Re = \sqrt{\frac{Inertia\ forces}{Viscous\ forces}} = \frac{\rho\ u\ d}{\mu} \tag{9}$$

Where the distance (d) can be the length in the case of a flat plate, the diameter in the case of a circumferential tube, or the hydraulic diameter (D_h) in the case of higher complexity geometries.

$$D_h = \frac{4\ A}{P} \tag{10}$$

Where A is the is the cross-sectional area and P is the wetted perimeter.

2.3.2 NUSSELT NUMBER:

Nusselt number (Nu) is one of the most important dimensionless numbers in terms of convection heat transfer because it is a measurement of the convection heat transfer occurring at the surface. There are two important facts to highlight: First, the Nusselt number is only dependent of the Reynolds number, Prandtl number and the dimensionless distance

(0,1). Second, if the Nusselt number is known, the heat transfer coefficient will be calculated straightforward.

$$Nu = \frac{h\,L}{k_{fluid}} \tag{11}$$

$$Nu = f(x^*, Re_L, \mathrm{Pr}) \tag{14}$$

Several approaches have been done to achieve Nusselt values for flat plate correlations. The most typical boundary conditions are uniform wall temperature (UWT) and uniform wall heat flux (UHF).

Local Nusselt number correlation for constant wall temperature for the laminar region at external forced flow:

$$Nu_x = 0.332\, Re_x^{\frac{1}{2}}\, Pr^{\frac{1}{3}} \tag{15}$$

Averaged:

$$\overline{Nu_L} = 0.664\, Re_L^{\frac{1}{2}}\, Pr^{\frac{1}{3}} \tag{16}$$

For $0.6 \leq \mathrm{Pr}$.

Local Nusselt number correlation for constant wall temperature for the turbulent region at external forced flow:

$$Nu_x = 0.0296\, Re_x^{\frac{4}{5}}\, Pr^{\frac{1}{3}} \tag{17}$$

For $0.6 \leq \mathrm{Pr} \leq 60$.

Averaged Nusselt number correlation for constant wall temperature for the turbulent region at external forced flow [11]:

$$Nu_L = 0.037\, Re_L^{\frac{4}{5}}\, Pr^{\frac{1}{3}} \tag{18}$$

For $0.6 \leq \text{Pr} \leq 60$, $5\ 10^5 \leq Re_L \leq 10^7$ and when the laminar region is depreciable.

Averaged Nusselt number correlation for constant wall temperature for the mixed region at external forced flow:

$$\overline{Nu_L} = \left(0.037\, Re_L^{\frac{4}{5}} - A\right) Pr^{\frac{1}{3}} \tag{19}$$

$$A = 0.037\, Re_{x,c}^{\frac{4}{5}} - 0.664\, Re_{x,c}^{\frac{1}{2}} \tag{20}$$

For $0.6 \leq \text{Pr} \leq 60$ and $Re_{x,c} \leq Re_L \leq 10^8$.

Moreover, a combination of upcoming and previous correlations can be done to determine the local Nusselt number taking in account the transition region [12].

$$Nu_{trans} = Nu_{lam}(Re_l, \text{Pr}) \left(\frac{Re_x}{Re_l}\right)^c \tag{21}$$

$$Re_l = 3.6\ 10^5 \left(\frac{100\, u_r'}{u_\infty}\right)^{-\frac{5}{4}} \tag{22}$$

$$c = 0.9922\, log_{10}\, Re_l - 3.013 \tag{23}$$

For $Re_l < 5\ 10^5$.

$$Nu_{turb} = \frac{Re_x \ \mathrm{Pr} \left(\frac{C_f}{2}\right)}{1 + 12.7 \left(Pr^{\frac{2}{3}} - 1\right) \sqrt{\frac{C_f}{2}}} \tag{24}$$

$$C_f = \frac{0.455}{[\ln(0.06 \ Re_x)]^2} \tag{25}$$

For gases can be simplified as:

$$Nu_{turb} = 0.0296 \ Re_x^{0.8} \ Pr^{0.6} \tag{26}$$

$$Nu_x = \left[Nu_{lam}^5 + (Nu_{trans}^{-10} + Nu_{turb}^{-10})^{-\frac{1}{2}}\right]^{\frac{1}{5}} \tag{27}$$

Nusselt number correlation for internal flow in circular tubes for the turbulent region for both UHF and UWT:

$$Nu_D = \frac{(f/8) \ (Re_D - 1000) \ Pr}{1 + 12.7 \ (f/8)^{\frac{1}{2}} \left(Pr^{\frac{2}{3}} - 1\right)} \tag{28}$$

For $0.5 \leq \mathrm{Pr} \leq 2000$ and $3000 \leq Re_D \leq 5 \ 10^6$.

$$f = (0.79 \ln Re_D - 1.64)^{-2} \tag{29}$$

For $3000 \leq Re_D \leq 5 \ 10^6$.

As the properties of the fluid are going to vary significantly, it is important to make some corrections. The correlations for external flow must be evaluated at the freestream

temperature (T_∞) and result multiplied by the absolute temperature ratio $(T_w / T_\infty)^{-n}$, with n in the range of 0.25 to 0.4. [12]

2.3.3 PRANDTL NUMBER:

Prandtl number is a dimensionless number only dependent on the fluid properties as the ratio of momentum (kinematic viscosity) and thermal diffusivity.

$$Pr = \frac{\nu}{\alpha} \tag{30}$$

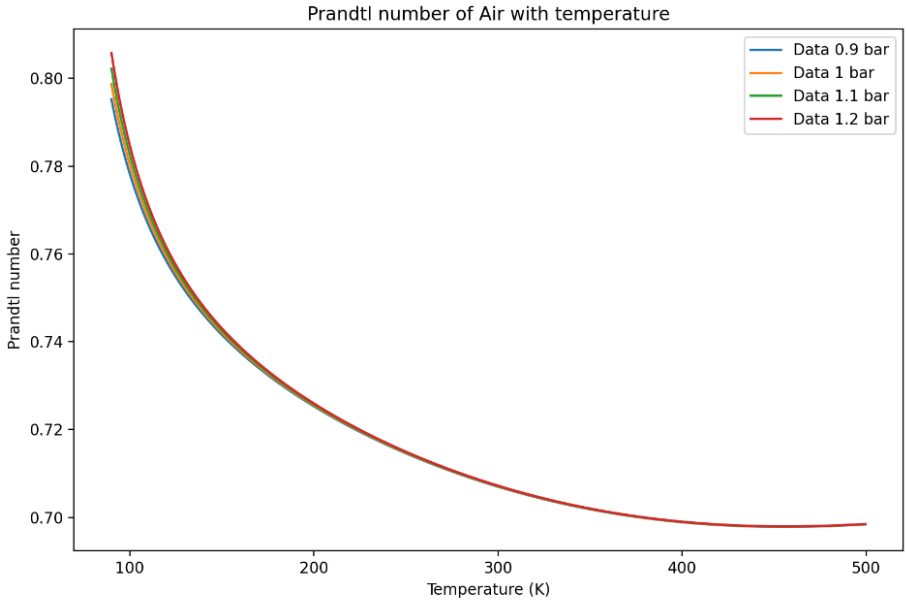

Figure 12: Prandtl number variation with temperature and pressure data.

2.4 THE THERMAL RESISTANCE METHOD:

For some simple cases with one-dimensional conduction through a wall with no heat generation and constant properties, temperature varies linearly with the perpendicular direction. Thereby, the Fourier's law can be simplified.

$$q''_x = -k\frac{dT}{dx} = \frac{k}{L}\left(T_{s,1} - T_{s,2}\right) \tag{31}$$

$$q_x = q''_x\, A = \frac{k\, A}{L}\left(T_{s,1} - T_{s,2}\right) \tag{32}$$

A similitude with electrical resistance is coming up where temperature is equal to voltage, heat flux is equal to intensity and the resistance will vary depending on the heat transfer method.

$$\frac{E_{s,1} - E_{s,2}}{I} = R_e \rightarrow \frac{T_{s,1} - T_{s,2}}{q_x} = R_t \tag{33}$$

Thermal resistance for conduction:

$$R_{t,cond} = \frac{L}{k\, A} \tag{34}$$

Thermal resistance for convection:

$$R_{t,conv} = \frac{1}{h\, A} \tag{35}$$

Thermal resistance for radiation:

$$R_{t,rad} = \frac{1}{h_{\,r} A} \tag{36}$$

For a case where there is a hot fluid at a temperature $T_{\infty,1}$ flowing in one side of a wall with a thermal conductivity k and a cold fluid at a temperature $T_{\infty,2}$, there will be a temperature in the hot surface of the wall $T_{s,1}$ and a temperature in the cold surface of the wall $T_{s,2}$. As there is a temperature difference, a heat flux will be developed and a variation of temperature along the network, as seen in Figure 15.

As the heat flux is constant through the whole network, these resistances can be grouped and form a whole equation for the problem.

Sometimes can be needed to have a guess initial value and apply an iteration method to reach a feasible solution.

$$q_x = \frac{T_{\infty,1} - T_{\infty,2}}{R_{total}} \tag{37}$$

$$R_{total} = \frac{1}{h_1\, A} + \frac{L}{k\, A} + \frac{1}{h_2\, A} \tag{38}$$

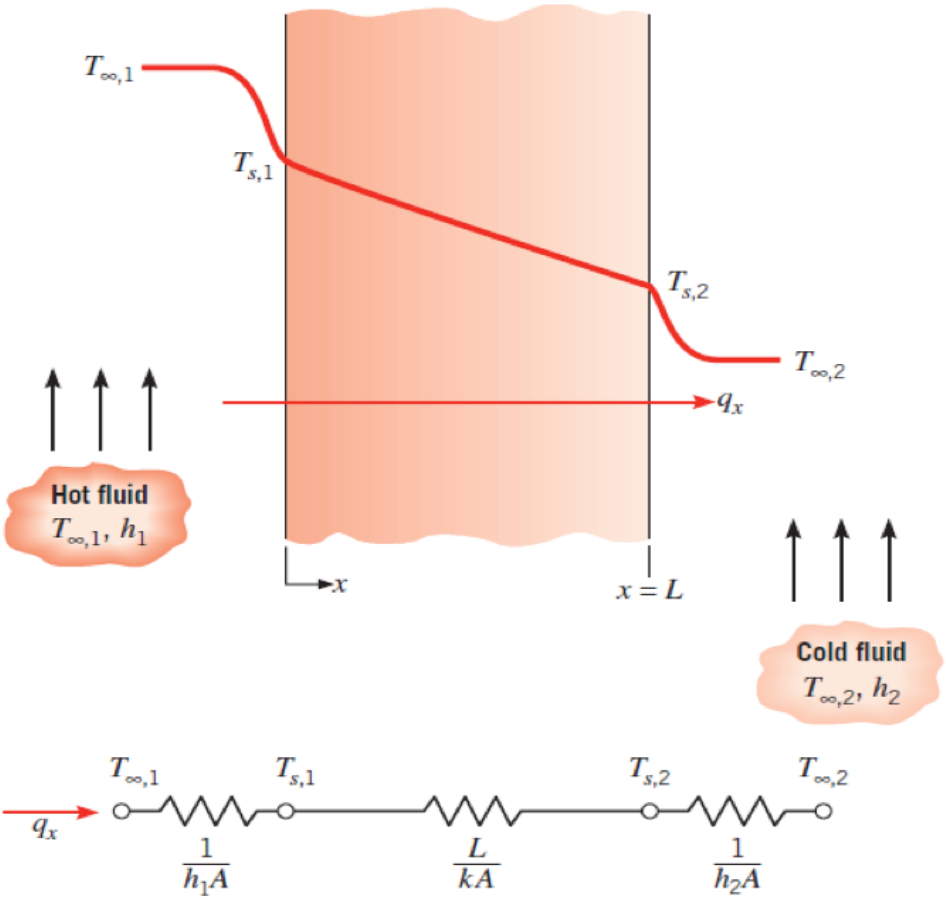

Figure 13: Heat transfer through the wall and the resistance equivalent [8]

2.5 GOVERNING EQUATIONS:

ANSYS CFX [5] will try to solve by iterations the main equations that model the heat and mass transfer over the whole network. These equations are for a stationary frame and instantaneous and then averaged due to different turbulent models then explained. [13].

The continuity equation to ensure that mass is conserved:

$$\frac{\partial \rho}{\partial t} + \nabla \cdot (\rho \, \boldsymbol{U}) = 0 \tag{39}$$

The momentum equation:

$$\frac{\partial (\rho \, \boldsymbol{U})}{\partial t} + \nabla \cdot (\rho \, \boldsymbol{U} \otimes \boldsymbol{U}) = -\nabla \mathrm{p} + \nabla \cdot \tau + \boldsymbol{S}_M \tag{40}$$

$$\tau = \mu \left(\nabla \boldsymbol{U} + (\nabla \boldsymbol{U})^T - \frac{2}{3} \, \delta \, \nabla \cdot \boldsymbol{U} \right) \tag{41}$$

The total enthalpy equation:

$$\frac{\partial (\rho \, h_{tot})}{\partial t} - \frac{\partial p}{\partial t} + \nabla \cdot (\rho \, \boldsymbol{U} \, h_{tot}) = \nabla \cdot (\lambda \, \nabla \mathrm{T}) + \nabla \cdot (\boldsymbol{U} \cdot \tau) + \boldsymbol{U} \cdot \boldsymbol{S}_M + \boldsymbol{S}_E \tag{42}$$

$$h_{tot} = h + \frac{1}{2} \, \boldsymbol{U^2} \tag{43}$$

2.5.1 REYNOLDS AVERAGED NAVIER-STOKES EQUATIONS:

At first it might seem that solving the equations with sufficient power is possible. Actually, in turbulent flows the length scale would be so small that it would not be possible to compute it on the mesh. Here is where turbulence models appear to have solution to the problems without having direct numerical simulation and an extremely fine mesh.

Looking at huge timescales in turbulent fluctuations, can be identified an average component and a fluctuating component. In order to reduce the computational effort, in the Navier-Stokes equations these components are introduced to produce the Reynolds Averaged Navier-Stokes (RANS) equations [26]. For example, the velocity can be divided as:

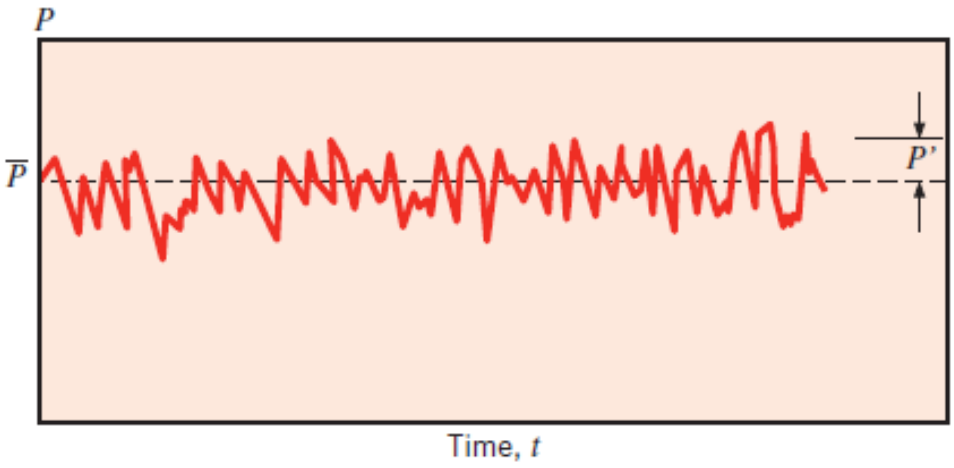

Figure 14: Turbulent variable divided into an average and fluctuating components.

$$U_i = \overline{U}_\iota + u_i \tag{44}$$

$$\overline{U}_\iota = \frac{1}{\Delta t} \int_t^{t+\Delta t} U_i \, dt \tag{45}$$

For compressible flows, the averaging is weighted by density (Favre-averaging).

The following equations are the governing equations substituting the averaged components:

$$\frac{\partial \rho}{\partial t} + \frac{\partial}{\partial x_j}(\rho\, U_j) = 0 \tag{46}$$

$$\frac{\partial(\rho\, U_i)}{\partial t} + \frac{\partial}{\partial x_i}(\rho\, U_i\, U_j) = -\frac{\partial p}{\partial x_i} + \frac{\partial}{\partial x_j}(\tau_{ij} - \rho\, \overline{u_i u_j}) + \boldsymbol{S}_M \tag{47}$$

$$\frac{\partial(\rho\, h_{tot})}{\partial t} - \frac{\partial p}{\partial t} + \frac{\partial}{\partial x_j}(\rho\, U_j\, h_{tot}) = \frac{\partial}{\partial x_j}\left(\lambda \frac{\partial T}{\partial x_j} - \rho\, \overline{u_j h}\right) + \frac{\partial}{\partial x_j}\left[U_i(\tau_{ij} - \rho\, \overline{u_i u_j})\right] + \boldsymbol{S}_E \tag{48}$$

$$h_{tot} = h + \frac{1}{2}\, U_i\, U_j + k \tag{49}$$

$$U_i\, k = \frac{1}{2}\overline{u_i^2} \tag{50}$$

2.5.2 EDDY VISCOSITY TURBULENCE MODELS:

These models [27] propose that turbulence are small eddies that are continuously forming and dissipating, and Reynolds stresses are related with the mean velocity gradients and eddy (turbulent) viscosity by the gradient diffusion hypothesis as:

$$\frac{\partial(\rho\, U_i)}{\partial t} - \rho\, \overline{u_i u_j} = \mu_t \left(\frac{\partial U_i}{\partial x_j} + \frac{\partial U_j}{\partial x_i}\right) - \frac{2}{3}\, \delta_{ij} \left(\rho\, k + \mu_t\, \frac{\partial U_k}{\partial x_k}\right) \tag{51}$$

Where μ_t is the turbulent viscosity, that should be known.

The eddy diffusivity hypothesis states that Reynolds fluxes of a scalar are linearly related to the mean scalar gradient:

$$-\rho\, \overline{u_i \varphi} = \Gamma_t\, \frac{\partial \Phi}{\partial x_i} \tag{52}$$

Where Γ_t is the eddy diffusivity:

$$\Gamma_t = \frac{\mu_t}{Pr_t} \tag{53}$$

Where Pr_t is the turbulent Prandtl number.

With this configuration, the Reynolds averaged momentum and scalar transport equation becomes:

$$\frac{\partial \rho\, U_i}{\partial t} + \frac{\partial}{\partial x_j}\left(\rho\, U_i\, U_j\right) = -\frac{\partial p'}{\partial x_i} + \frac{\partial}{\partial x_j}\left[\mu_{eff}\left(\frac{\partial U_i}{\partial x_j} + \frac{\partial U_j}{\partial x_i}\right)\right] + \boldsymbol{S}_M \tag{54}$$

Where $\boldsymbol{S}_M$ is the body forces' sum, p' is the modified pressure and μ_{eff} the effective viscosity:

$$\mu_{eff} = \mu + \mu_t \tag{55}$$

$$p' = p + \frac{2}{3}\rho\, k + \frac{2}{3}\mu_{eff}\,\frac{\partial U_k}{\partial x_k} \tag{56}$$

The Reynolds averaged energy equation becomes:

$$\frac{\partial(\rho\, h_{tot})}{\partial t} - \frac{\partial p}{\partial t} + \frac{\partial}{\partial x_j}\left(\rho\, U_j\, h_{tot}\right) = \frac{\partial}{\partial x_j}\left(\lambda\frac{\partial T}{\partial x_j} + \frac{\mu_t}{Pr_t}\frac{\partial h}{\partial x_j}\right) + \frac{\partial}{\partial x_j}\left[U_i\left(\tau_{ij} - \rho\,\overline{u_i u_j}\right)\right] + \boldsymbol{S}_E \tag{57}$$

The Reynolds averaged transport equation for addition variables becomes:

$$\frac{\partial\, \rho\, \Phi}{\partial t} + \frac{\partial}{\partial x_j}\left(\rho\, U_j\, \Phi\right) = \frac{\partial}{\partial x_j}\left[\left(\Gamma_\Phi + \frac{\mu_t}{\sigma_\Phi}\right)\frac{\partial \Phi}{\partial x_j}\right] + \boldsymbol{S}_\Phi \tag{58}$$

2.5.3 TWO EQUATION TURBULENCE MODELS:

The term 'Two equation' is due to velocity and length scale are determinate by two different transport equations. The gradient diffusion hypothesis is used in two-equation models to connect Reynolds stresses to mean velocity gradients and turbulent viscosity. The product of a turbulent velocity and a turbulent length scale is used to simulate turbulent viscosity. The turbulent kinetic energy, which is obtained by solving its transport equation, is used to calculate the turbulence velocity scale. Two parameters of the turbulence field, generally the turbulent kinetic energy and its dissipation rate, are used to determine the turbulent length scale. The solution of its transport equation yields the turbulent kinetic energy dissipation rate.

2.5.3.1 THE K-EPSILON MODEL :

The k (turbulence kinetic energy) $[m^2/s^2]$ is the variance of the fluctuations in velocity and ε (turbulence eddy dissipation) $[m^2/s^3]$ [28]. This model results quite accurate for flow far from the wall. With the introduction of this new variables, the current equations are Equation 46, Equation 54 and Equation 55 and the addition of the relation between turbulence viscosity and turbulence kinetic energy by:

$$\mu_t = C_\mu \, \rho \, \frac{k^2}{\varepsilon} \tag{59}$$

Where C_μ is a constant with value 0.09.

The values of the new variables k and ε come form differential transport equation for the turbulence kinetic energy and turbulence dissipation rate:

$$\frac{\partial(\rho\, k)}{\partial t} + \frac{\partial}{\partial x_j}(\rho\, U_j\, k) = \frac{\partial}{\partial x_j}\left[\left(\mu + \frac{\mu_t}{\sigma_k}\right)\frac{\partial k}{\partial x_j}\right] + P_k - \rho\, \varepsilon + P_{kb} \tag{60}$$

$$\frac{\partial(\rho\, \varepsilon)}{\partial t} + \frac{\partial}{\partial x_j}(\rho\, U_j\, \varepsilon) = \frac{\partial}{\partial x_j}\left[\left(\mu + \frac{\mu_t}{\sigma_\varepsilon}\right)\frac{\partial \varepsilon}{\partial x_j}\right] + \frac{\varepsilon}{k}(C_{\varepsilon 1} P_k - C_{\varepsilon 2}\, \rho\, \varepsilon + C_{\varepsilon 1} P_{\varepsilon b}) \tag{61}$$

Where $C_{\varepsilon 1} = 1.44$, $C_{\varepsilon 2} = 1.92$, $\sigma_k = 1$, $\sigma_\varepsilon = 1.3$ are constants; P_k is the turbulence production due to viscous forces; P_{kb} and $P_{\varepsilon b}$ represents the influence of buoyancy forces.

$$P_k = \mu_t \left(\frac{\partial U_i}{\partial x_j} + \frac{\partial U_j}{\partial x_i}\right)\frac{\partial U_i}{\partial x_j} - \frac{2}{3}\frac{\partial U_k}{\partial x_k}\left(3\, \mu_t \frac{\partial U_k}{\partial x_k} + \rho\, k\right) \tag{62}$$

$$P_{\varepsilon b} = C_3 \cdot \max(0, P_{kb}) \tag{63}$$

If the buoyancy model is used:

$$P_{kb} = -\frac{\mu_t}{\rho\,\sigma_\rho}\,g_i\,\frac{\partial \rho}{\partial x_i} \tag{64}$$

If the Boussinesq buoyancy model is used:

$$P_{kb} = \frac{\mu_t}{\rho\,\sigma_\rho}\,\rho\,\beta\,g_i\,\frac{\partial T}{\partial x_i} \tag{65}$$

With default constant values of turbulence Schmidt number (σ_ρ) of 0.9 for Boussinesq buoyancy and 1 for buoyancy model and dissipation coefficient (C_3) of 1.

2.5.3.2 THE K-OMEGA MODEL :

k-epsilon models usually need a high-resolution mesh near the wall (over $y^+ < 0.2$), in comparison with k-omega, developed by Wilcox [29], models that needs at least $y^+ < 2$ which is more achievable. Moreover, this model more solid than the previous k-epsilon model near the wall. Turbulent viscosity is related with turbulent kinetic energy and turbulent frequency by:

$$\mu_t = \rho\,\frac{k}{\omega} \tag{66}$$

The k (turbulence kinetic energy) and ω (turbulent frequency) can be obtained by:

$$\frac{\partial(\rho\,k)}{\partial t} + \frac{\partial}{\partial x_j}(\rho\,U_j\,k) = \frac{\partial}{\partial x_j}\left[\left(\mu + \frac{\mu_t}{\sigma_k}\right)\frac{\partial k}{\partial x_j}\right] + P_k - \beta'\,\rho\,k\,\omega + P_{kb} \tag{67}$$

$$\frac{\partial(\rho\,\omega)}{\partial t} + \frac{\partial}{\partial x_j}(\rho\,U_j\,\varepsilon) = \frac{\partial}{\partial x_j}\left[\left(\mu + \frac{\mu_t}{\sigma_\varepsilon}\right)\frac{\partial \omega}{\partial x_j}\right] + \alpha\,\frac{\omega}{k}\,P_k - \beta\,\rho\,\omega^2 + P_{\omega b} \tag{68}$$

$$-\rho\,\overline{u_i u_j} = \mu_t\left(\frac{\partial U_i}{\partial x_j}+\frac{\partial U_j}{\partial x_i}\right)-\frac{2}{3}\,\delta_{ij}\left(\rho\,k+\mu_t\frac{\partial U_k}{\partial x_k}\right) \tag{69}$$

P_k is calculated as in Equation 62; Buoyancy terms are the same as in Equations 64 and 65, with $\beta' = 0.09$, $\alpha = \frac{5}{9}$, $\beta = 0.075$, $\sigma_k = 2$, $\sigma_\omega = 2$; $P_{\omega b}$ as:

$$P_{\omega b} = \frac{\omega}{k}\left((\alpha+1)\,C_3\,\max(P_{kb},0)-P_{kb}\right) \tag{70}$$

2.5.3.3 THE SHEAR STRESS TRANSPORT (SST) MODEL:

To reduce some problems such as the strong sensitivity to freestream conditions or the high dependence sometimes of the specified ω at the inlet, a combination of $k-\omega$ model near the surface and $k-\varepsilon$ model in the outer regions is suggested [32]. This method is so accurate with adverse pressure gradients and makes a limiter to the eddy-viscosity formulation:

$$v_t = \frac{a_1\,k}{\max(a_1\,\omega\,,\;S\,F_2)} \tag{71}$$

$$v_t = \frac{\mu_t}{\rho} \tag{72}$$

Where F_2 is another blending function that restricts the limiter to the wall boundary layer; S is an invariant measure of the strain rate; and $\sigma_{k1} = 1.176$.

2.5.3.4 BLENDING FUNCTIONS:

They are based on the distance to the nearest surface and on the flow variables.

$$F_1 = \tanh(arg_1^4) \tag{73}$$

$$arg_1 = \min(\max\left(\frac{\sqrt{k}}{\beta' \, \omega \, y'}, \frac{500 \, \upsilon}{y^2 \, \omega}\right), \frac{4 \, \rho \, k}{CD_{k\omega} \, \sigma_{\omega 2} \, y^2}) \tag{74}$$

$$CD_{k\omega} = \max\left(2 \, \rho \frac{1}{\sigma_{\omega 2} \, \omega} \frac{\partial k}{\partial x_j} \frac{\partial \omega}{\partial x_j}, 10^{-10}\right) \tag{75}$$

$$F_2 = \tanh(arg_2^2) \tag{76}$$

$$arg_2 = \max\left(\frac{2\sqrt{k}}{\beta' \, \omega \, y'}, \frac{500 \, \upsilon}{y^2 \, \omega}\right) \tag{77}$$

Where y is the distance to the nearest wall and υ is the kinematic viscosity.

2.5.4 LAMINAR-TURBULENT TRANSITION MODEL: TWO EQUATION GAMMA THETA TRANSITION MODEL

As said before, there are 3 main regions in the fluid flow, and to model the laminar and transition region there are two main models: the One Equation Intermittency Model and the Two Equation Gamma Theta Transition Model [30], which is the recommended transition model for general purpose which uses one equation for the intermittency and another the transition onset criteria. For the last and used model, to calculate the transitional boundary layer the mesh must have $1 < y^+$.

The transport equation for the intermittency (γ):

$$\frac{\partial(\rho\,\gamma)}{\partial t} + \frac{\partial(\rho\,U_j\,\gamma)}{\partial x_j} = P_{\gamma 1} - E_{\gamma 1} + P_{\gamma 2} - E_{\gamma 2} + \frac{\partial}{\partial x_j}\left[\left(\mu + \frac{\mu_t}{\sigma_\gamma}\right)\frac{\partial \gamma}{\partial x_j}\right] \tag{78}$$

$$P_{\gamma 1} = 2\,F_{length}\,\rho\,S\,[\gamma\,F_{onset}]^{C_{\gamma 3}} \tag{79}$$

$$E_{\gamma 1} = P_{\gamma 1}\,\gamma \tag{80}$$

$$P_{\gamma 2} = (2\,c_{\gamma 1})\rho\,\Omega\,\gamma\,F_{turb} \tag{81}$$

$$E_{\gamma 2} = c_{\gamma 2}\,P_{\gamma 2}\,\gamma \tag{82}$$

Where $c_{\gamma 1} = 0.03$, $c_{\gamma 2} = 50$, $c_{\gamma 3} = 0.5$, $\sigma_\gamma = 1.0$, S is the strain rate magnitude, Ω is the magnate of vorticity rate and F_{length} is an empirical correlation that controls the length of the transition region.

The transition onset is controlled by:

$$Re_v = \frac{\rho\, y^2\, S}{\mu} \tag{83}$$

$$R_T = \frac{\rho\, k}{\mu\, \omega} \tag{84}$$

$$F_{onset1} = \frac{Re_v}{2.193\, Re_{\theta c}} \tag{85}$$

$$F_{onset2} = \min(\max(F_{onset1}, {F_{onset1}}^4), 2.0) \tag{86}$$

$$F_{onset3} = \max\left(1 - \left(\frac{R_T}{2.5}\right)^3, 0\right) \tag{87}$$

$$F_{onset} = \max(F_{onset2} - F_{onset3}, 0) \tag{88}$$

$$F_{turb} = e^{-\left(\frac{R_T}{4}\right)^4} \tag{89}$$

Where $Re_{\theta c}$ is the critical Reynolds number where the intermittency first starts to increase in the boundary layer.

The transport equation for the transition momentum thickness Reynolds number ($\widetilde{Re_{\theta t}}$) is:

$$\frac{\partial(\rho\,\widetilde{Re_{\theta t}})}{\partial t}+\frac{\partial(\rho\,U_j\,\widetilde{Re_{\theta t}})}{\partial x_j}=P_{\theta t}+\frac{\partial}{\partial x_j}\left[\sigma_{\theta t}\left((\mu+\mu_t)\frac{\partial(\widetilde{Re_{\theta t}})}{\partial x_j}\right)\right] \tag{90}$$

$$P_{\theta t}=c_{\theta t}\,\frac{\rho}{t}\,(Re_{\theta t}-\widetilde{Re_{\theta t}})(1.0-F_{\theta t}) \tag{91}$$

$$t=\frac{500\,\mu}{\rho\,U^2} \tag{92}$$

$$F_{\theta t}=\min(\max\left(F_{wake}\,e^{-\left(\frac{y}{\delta}\right)^4},1.0-\left(\frac{\gamma-\frac{1}{50}}{1.0-\frac{1}{50}}\right)^2\right),1.0) \tag{93}$$

$$\theta_{BL}=\frac{\mu\,\widetilde{Re_{\theta t}}}{\rho\,U} \tag{94}$$

$$\delta_{BL}=\frac{15}{2}\,\theta_{BL} \tag{95}$$

$$\delta=\frac{50\,\Omega\,y}{U}\,\delta_{BL} \tag{96}$$

$$Re_{\omega} = \frac{\rho\ \omega\ y^2}{\mu} \tag{97}$$

$$F_{wake} = e^{-\left(\frac{Re_{\omega}}{10^5}\right)^2} \tag{98}$$

Where $c_{\theta t} = 0.03$, $\sigma_{\theta t} = 2.0$ and $Re_{\theta t}$ is the transition onset calculated as:

$$Re_{\theta t} = \begin{cases} \left[1173.51 - 589.428\ Tu + \frac{0.2196}{Tu^2}\right] F(\lambda_\theta), & Tu \leq 1.3 \\ 331.50\ [Tu - 0.5658]^{-0.671}\ F(\lambda_\theta), & Tu > 1.3 \end{cases} \tag{99}$$

$$F(\lambda_\theta) = \begin{cases} 1 - [-12.986\ \lambda_\theta - 123.66\ \lambda_{\theta^2} - 405.689\ \lambda_{\theta^3}]\ e^{-\left[\frac{Tu}{1.5}\right]^{1.5}}, & \lambda_\theta \leq 0 \\ 1 + 0.275\ \left[1 - e^{-35.0\ \lambda_\theta}\right] e^{\frac{-Tu}{0.5}}, & \lambda_\theta > 0 \end{cases} \tag{100}$$

$$\lambda_\theta = \left(\frac{\theta^2}{v}\right) \frac{dU}{ds} \tag{101}$$

Where Tu is the local turbulence intensity, λ_θ is the Thwaites pressure gradient coefficient and $\frac{dU}{ds}$ is the acceleration in the streamwise direction.

The length of the transition zone (F_{length}) is calculated with a modification to avoid a sharp increase in the skin friction in the boundary layer shortly after transition:

$$F_{length} = \begin{cases} \begin{bmatrix} 398.189E-1+(-119.270E-4)\widetilde{Re_{\theta t}} \\ +(-132.567E-6)\widetilde{Re_{\theta t}}^{2} \end{bmatrix}, \widetilde{Re_{\theta t}} < 400 \\ \begin{bmatrix} 263.404+(-123.939E-2)\widetilde{Re_{\theta t}}+ \\ (194.548E-5)\widetilde{Re_{\theta t}}^{2}+(-101.695E-8)\widetilde{Re_{\theta t}}^{3} \end{bmatrix}, 400 \le \widetilde{Re_{\theta t}} < 596 \\ \left[0.5-\left(\widetilde{Re_{\theta t}}-596.0\right)3.0E-4\right], \ 596 \le \widetilde{Re_{\theta t}} < 1200 \\ [0.3188], \ 1200 \le \widetilde{Re_{\theta t}} \end{cases} \quad (102)$$

$$F_{sublayer} = e^{-\left(\frac{R_\omega}{0.4}\right)^2} \quad (103)$$

$$R_\omega = \frac{\rho\, y^2\, \omega}{500\, \mu} \quad (104)$$

$$F_{length} = F_{length}\left(1 - F_{sublayer}\right) + 40.0\, F_{sublayer} \quad (105)$$

$Re_{\theta c}$ is the point where the model is activated to match $Re_{\theta t}$ and F_{length}. $Re_{\theta c}$ is where turbulence starts to grow and $Re_{\theta t}$ is where the velocity profile starts a turbulence behavior.

$$Re_{\theta c} = \begin{cases} \begin{bmatrix} \widetilde{Re_{\theta t}} - (396.035\ 10^{-2}) + (-120.656\ 10^{-4})\widetilde{Re_{\theta t}} \\ +(868.230\ 10^{-6})Re_{\theta t^2} + (-696.506\ 10^{-9})Re_{\theta t^3} \\ +(174.105\ 10^{-12})Re_{\theta t^4} \end{bmatrix}, \widetilde{Re_{\theta t}} \le 1870 \\ \left[\widetilde{Re_{\theta t}} - \left(593.11 + \left(\widetilde{Re_{\theta t}} - 1870.0\right)0.482\right)\right], \widetilde{Re_{\theta t}} > 1870 \end{cases} \quad (106)$$

Interaction with SST model:

$$\frac{\partial}{\partial t}(\rho\, k) + \frac{\partial}{\partial x_j}(\rho\, u_j\, k) = \widetilde{P_k} - \widetilde{D_k} + \frac{\partial}{\partial x_j}\left((\mu + \sigma_k\, \mu_t)\frac{\partial k}{\partial x_j}\right) \quad (107)$$

$$\widetilde{P_k} = \gamma_{eff}\, P_k \tag{108}$$

$$\widetilde{D_k} = \min(\max(\gamma_{eff}, 0.1), 1.0)\, D_k \tag{109}$$

$$R_y = \frac{\rho\, y \sqrt{k}}{\mu} \tag{110}$$

$$F_3 = e^{-\left(\frac{R_y}{120}\right)^8} \tag{111}$$

$$F_1 = \max(F_{1orig}, F_3) \tag{112}$$

Where P_k, F_{1orig} and D_k are from the original SST model.

2.5.5 Y+:

As said before, the boundary layer rises when it gets close to a wall. The variation of the variables in the near-wall region use to high so, it is important to catch this phenomenon to accurate study the heat transfer. y^+ is a dimensionless parameter related with the distance between the surface wall and the first mesh cell.

$$y^+ = \frac{u^* y}{\upsilon} \tag{113}$$

$$u^* = \sqrt{\frac{\tau_w}{\rho}} \tag{114}$$

Where u^* is the friction velocity, y is the wall normal coordinate, υ is the kinematic viscosity, τ_w is the wall shear and ρ the density. [15].

The different sub-layers over the near-wall region have different accuracy of y^+ according to [16], but depending on the Turbulence model used, a higher or lower y^+ can be needed:

-Viscous sub-layer: $0 < y^+ < 5$.

-Buffer layer: $5 < y^+ < 30$.

-Inertial sub-layer: $30 < y^+ < 200$.

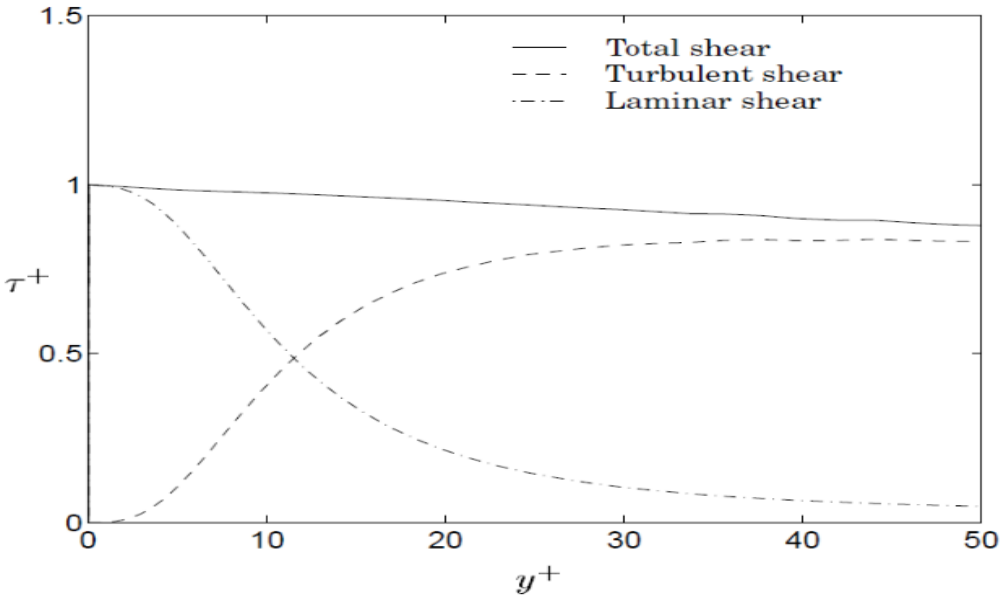

Figure 15: Laminar and turbulent shear in the near-wall region [15]

In the viscous sub-layer, that is the one on interest since is the one most near to the wall, the following equations are valid noting that they are normalized functions:

$$U^+ = y^+ \tag{115}$$

$$T^+ = Pr\, y^+ \tag{116}$$

$$k^+ = 0.1\, y^{+2} \tag{117}$$

$$\varepsilon^+ = 0.2 \tag{118}$$

2.5.6 FLAT PLATE VERIFICATION:

To verify the previous turbulence models, they will be run over the simplest geometry, a flat plate, and compare the results of the simulation with the outcome of the correlations.

The simulation's workflow will be explained more in detail in Chapter 5 for a more complex situation. For this simple case, a general guide is done.

For geometry, a simple flat plate was done by Pointwise [31] with a longitude of $0.31\ m$, just a layer of width, and same height as longitude but it is only necessary a height to let the flow achieve freestream conditions. Fluent can run 2D problems, but CFX only can run 3D geometries that is why is needed only a unique cell of width.

For mesh, it is computed a near-wall finer mesh (Figure 17) to achieve the heat transfer behavior; and also a refinement of the mesh were the flat plate starts, before there is a slip wall (adiabatic), to capture the transition between freestream and the flat plate (Figure 18).

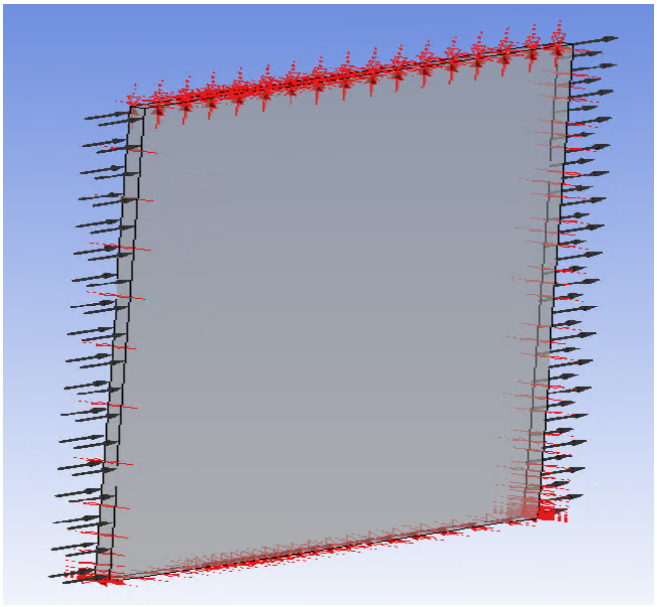

Figure 16: Flat Plate Geometry.

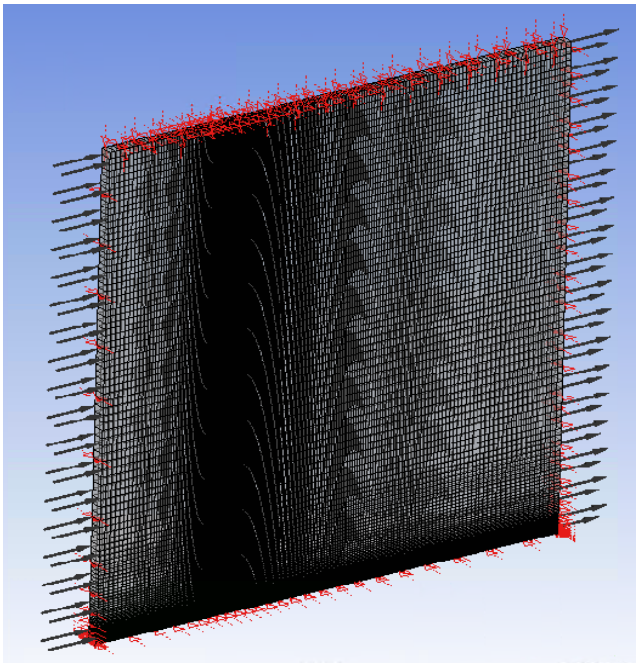

Figure 17: Flat Plate Mesh.

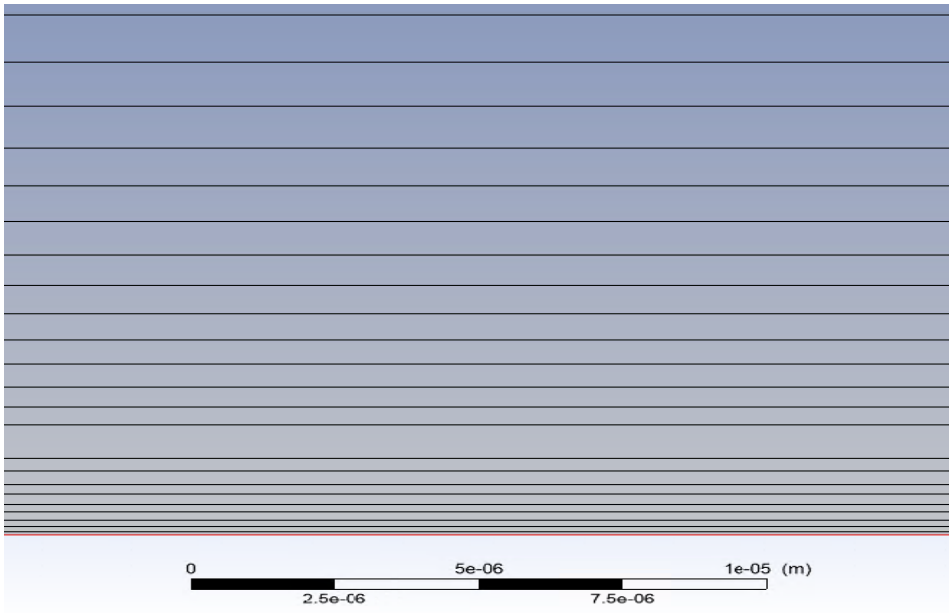

Figure 18:Flat Plate Near-Wall Refinement Mesh.

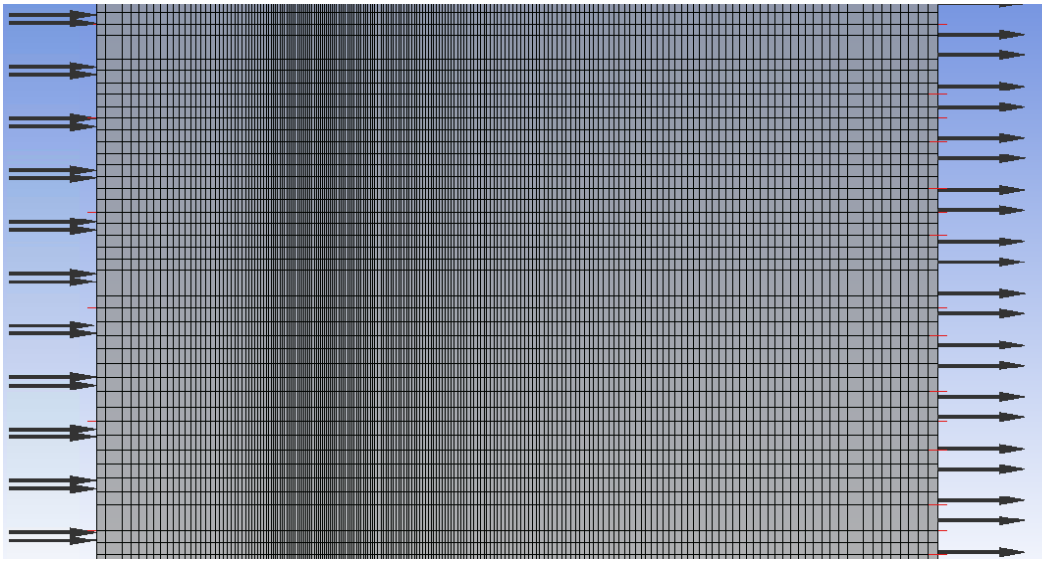

Figure 19: Flat Plate Starting Region Refinement Mesh.

For the boundaries, it is used the results from the whole simulation case to be able to compare it similar conditions such as the wall temperature or the inlet pressure. For the inlet it is used an 'Inlet' for 'Boundary Type', a 'Turbulence Intensity' of 0.037, a 'Relative Pressure' of $136274\ Pa$ and a 'Total Temperature' of $400.665\ K$. For the outlet it is used an 'Outlet' for 'Boundary Type', an 'Average Static Pressure' of $106810\ Pa$ with a deviation of 0.05 'Average Over Whole Outlet'. The wall is modeled as a 'Wall' 'Boundary Type' with a 'Temperature' of $91K$. The other boundaries such as the edges and the top are modeled as a 'Symmetry' in 'Boundary Type'.

Regarding other setup configuration, the material used is 'Air Ideal Gas' with the correspondent modifications. In relation with the model used, the 'Turbulence Numerics' is set to 'High Resolution', 'Heat Transfer' is selected as 'Total Energy', 'Turbulence' is 'Shear Stress Transport', and in the case of studying the laminar and transition region the 'Gamma Theta Model' is selected in the 'Transitional Turbulence' option.

The fully turbulent flat plate simulation finalizes with an average heat transfer coefficient of 709.551 $W/m^2\,K$, same for the correlations for different n factor results on 676.349 $W/m^2\,K$ for $n = -0.25$, 726.261 $W/m^2\,K$ for $n = -0.3$, and 779.911 $W/m^2\,K$ for $n = -0.35$. The local heat transfer coefficient is presented in Figure 19.

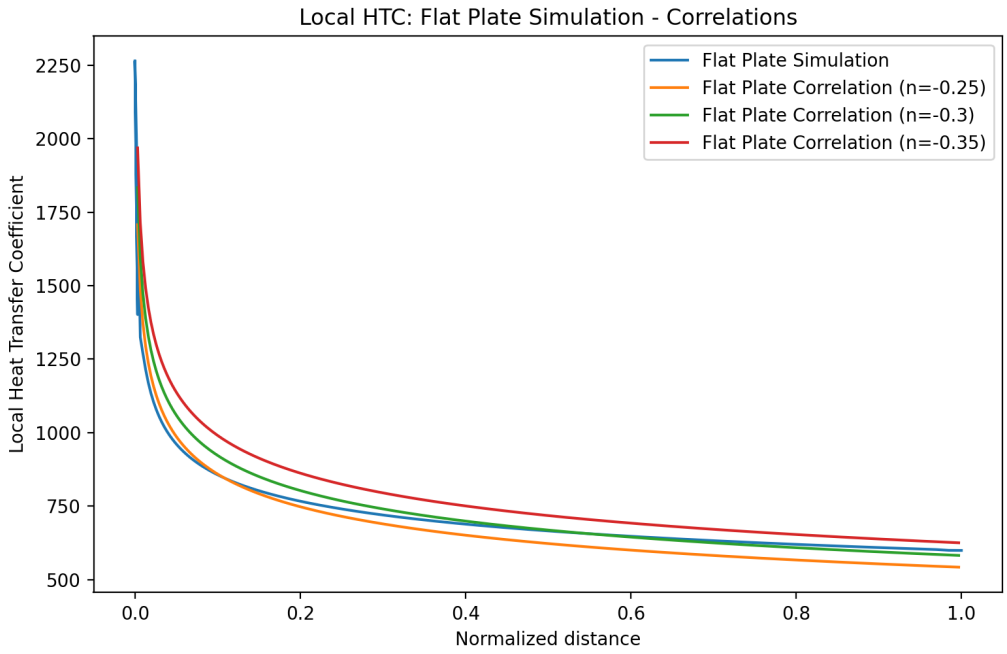

Figure 20: Local Turbulent Heat Transfer Coefficient Over The Flat Plate Compared With Correlations.

The transition flat plate case leads an average heat transfer coefficient of 655.227 $W/m^2\,K$, and correlations for different n factor results on 675.01 $W/m^2\,K$ for $n = -0.25$, 704.64 $W/m^2\,K$ for $n = -0.3$, and 757.62 $W/m^2\,K$ for $n = -0.35$. The local heat transfer coefficient is presented in Figure 20.

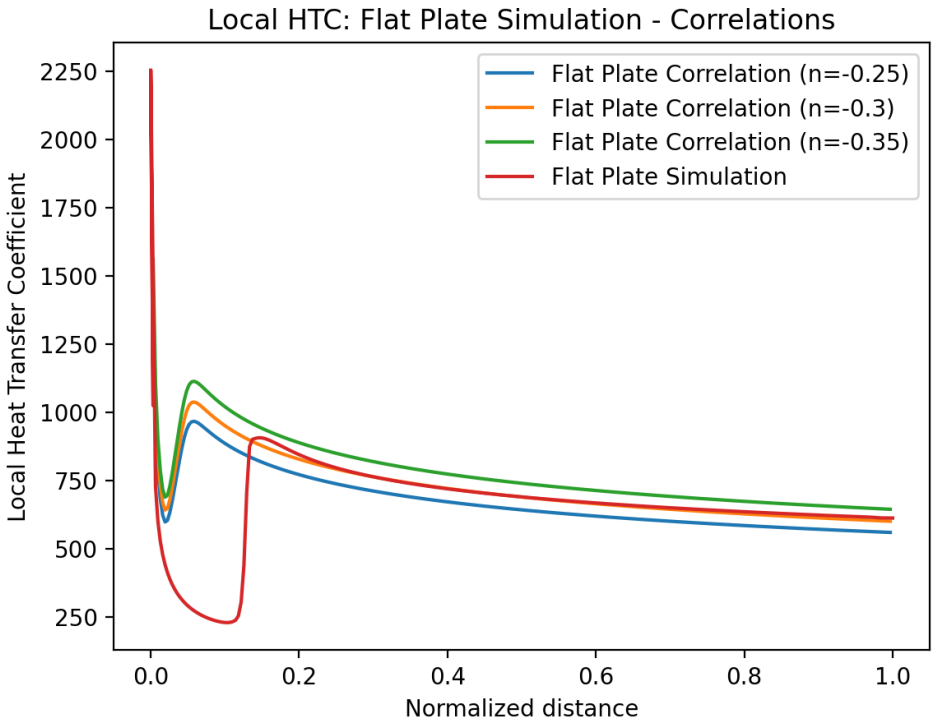

Figure 21: Local Transition Model Heat Transfer Coefficient Over The Flat Plate Compared With Correlations.

The fully turbulent model predicts overall well the heat transfer but with a difference of 3% in the average heat transfer coefficient for the $n = -0.3$ factor, that in each simulation seems that is the correct value for these measurements. Nevertheless, the correlations overpredicts the onset Reynolds number, that is only function of the inlet turbulence intensity. Furthermore, the flat plate predicts a huge sudden transition where this region is practically neglected, while the correlations result on an abrupt transition but not as snappish as the flat plate.

3 AIR PROPERTIES:

Governing equations are dependent on the fluid properties, the ones that are relevant to model for the heat transfer resolution are density (ρ), dynamic viscosity (μ), thermal conductivity (k), Prandtl number (Pr); other properties such as kinematic viscosity (ν) can be derived from the previous ones. Small temperature range between wall and freestream flow at normal conditions can lead in not a huge difference of data and the simulations can be easier. Working with air at high temperature difference (about 90K to 400K) leads on a significant variation of the solution that will be shown later. These properties are function of temperature and pressure.

The following correlations will be compared with data provided by CoolProp [14] that can be used by Python to see the effectiveness.

3.1 DYNAMIC VISCOSITY:

Dynamic viscosity is modelled by Sutherland's Formula based on an idealized intermolecular-force potential [10]:

$$\frac{\mu}{\mu_0} = \left(\frac{T}{T_0}\right)^c \left(\frac{T_0+S_\mu}{T+S_\mu}\right) \tag{120}$$

Where μ_0 is the reference viscosity, T_0 is the reference temperature and S_μ is the Sutherland constant. For air:

-$\mu_0 = 1.716\ 10^{-5}\ N \cdot s/m^2$.

-$T_0 = 273\ K$.

-$S_\mu = 111\ K$.

-$c = 1.5$.

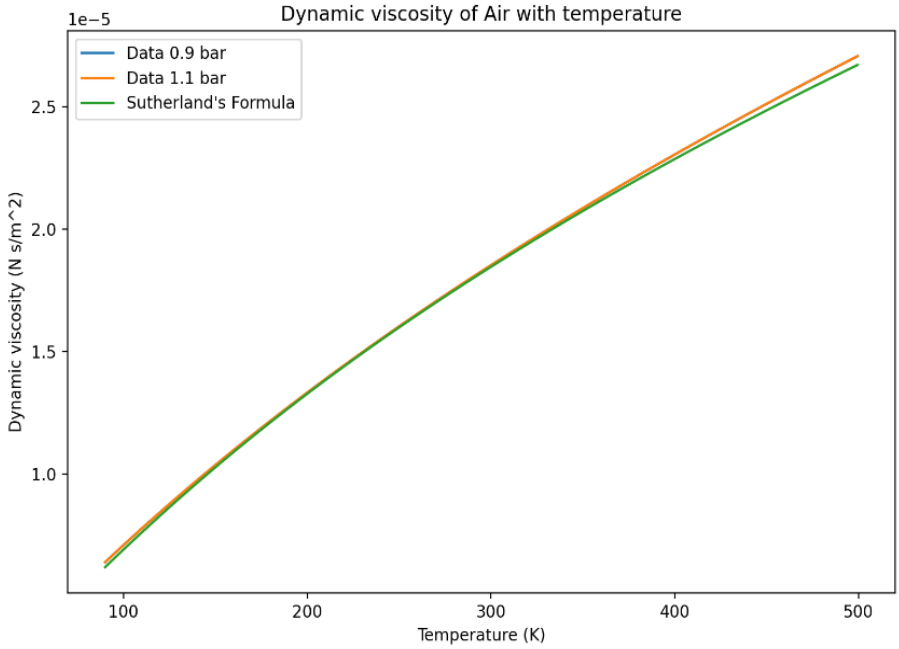

Figure 22: Dynamic viscosity variation with temperature with Sutherland's formula and pressure data.

Despite Sutherland's formula is only temperature dependent, it fits with the data that seems that there is no pressure dependency on the pressure range.

3.2 THERMAL CONDUCTIVITY:

Thermal conductivity can be modelled by Sutherland's formula as stated in Equation 4.

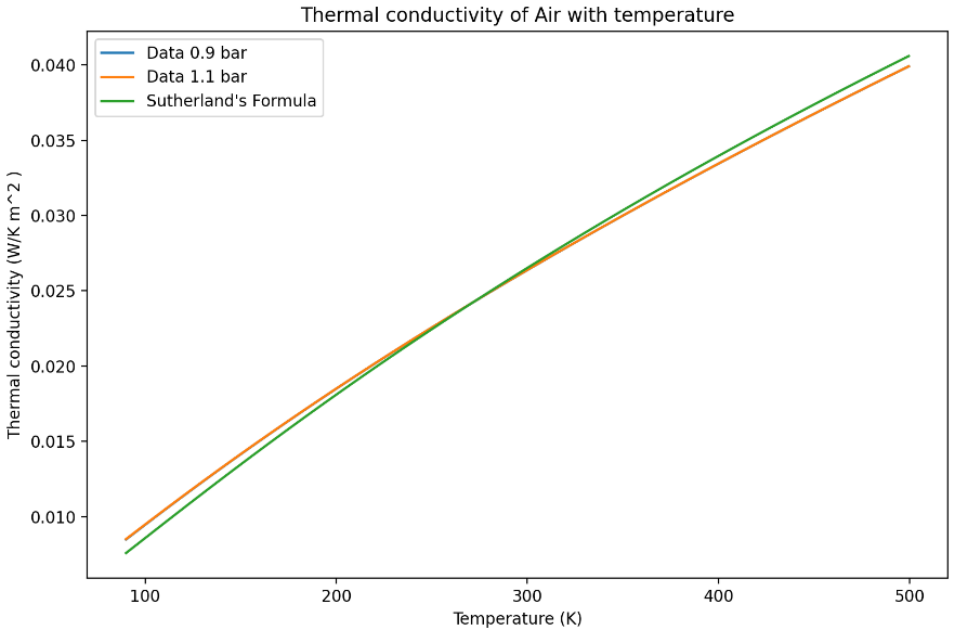

Figure 23: Thermal conductivity variation with temperature with Sutherland's formula and pressure data.

4 MATERIALS:

Previously, properties were presented as highly changeable at low temperatures.

Thermal conductivity is related with atoms' vibrations (speed of sound) that depends on phonons, electrons, and vacancies. Different materials thermal conductivity [17] are plotted below:

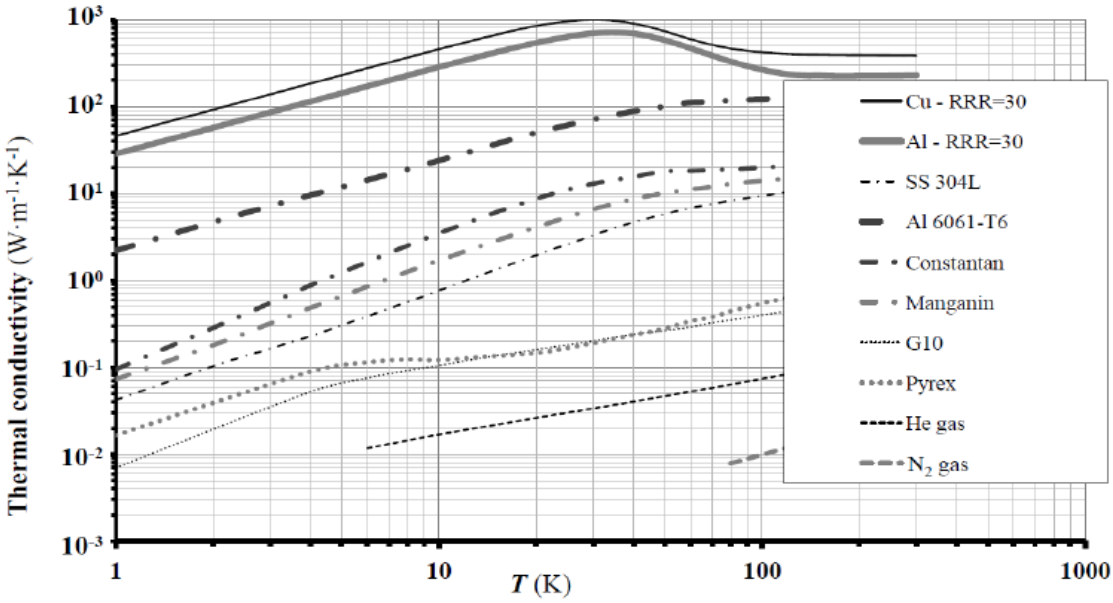

Figure 24: Thermal conductivity of various materials [17].

For pure metals, the electron energy transport (k_{el}) is the main contributor compared with phonon energy transport (k_{ph}) at any temperature. At very low temperatures, $k \propto T$. When T increases, impurities start to be taken in account and a maximum on the thermal conductivity is reached and is higher as higher purity is the material. This purity can be expressed by the Residual Resistive Ratio (RRR). In coppers, normal coppers have $5 < RRR < 150$, Oxygen-Free thermal Conductivity coppers (OFHC) have $100 < RRR < 200$, and very pure coppers have $200 < RRR < 5000$.

$$RRR = \frac{\rho\,(273\ K)}{\rho\,(0\ K)} \approx \frac{\rho\,(273\ K)}{\rho\,(4.2\ K)} \tag{121}$$

Where ρ is the electrical resistivity.

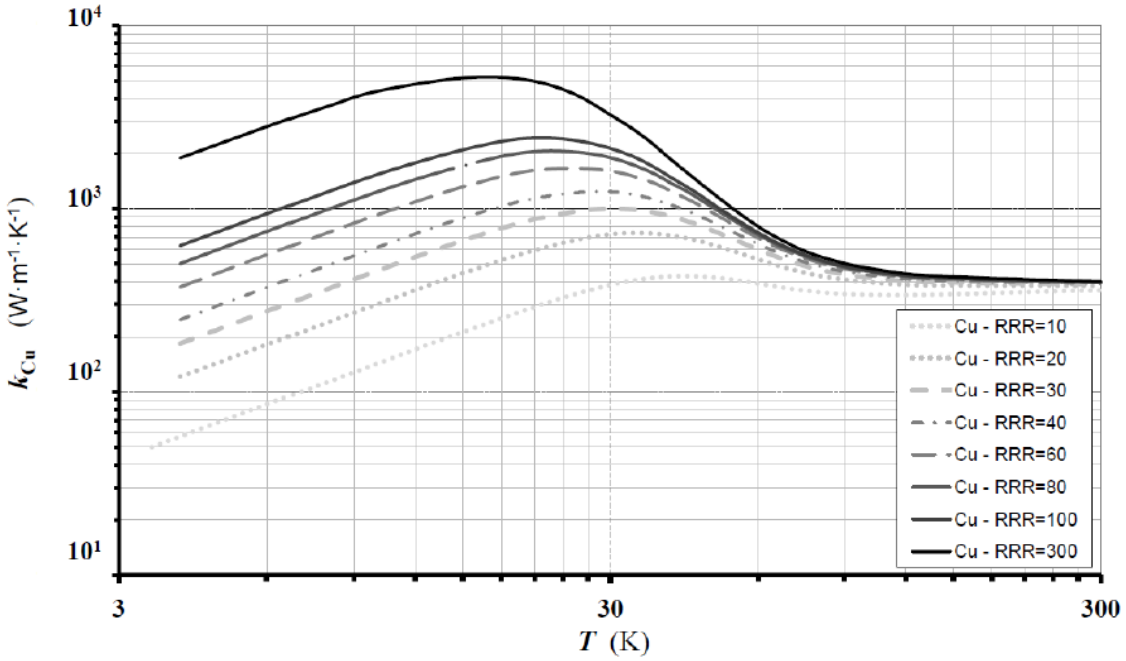

Figure 25: Copper thermal conductivity for different purity factors [17].

For non-pure metals and metallic alloys, both energy transport factors are comparable so thermal conductivity is approximately linear at low temperatures.

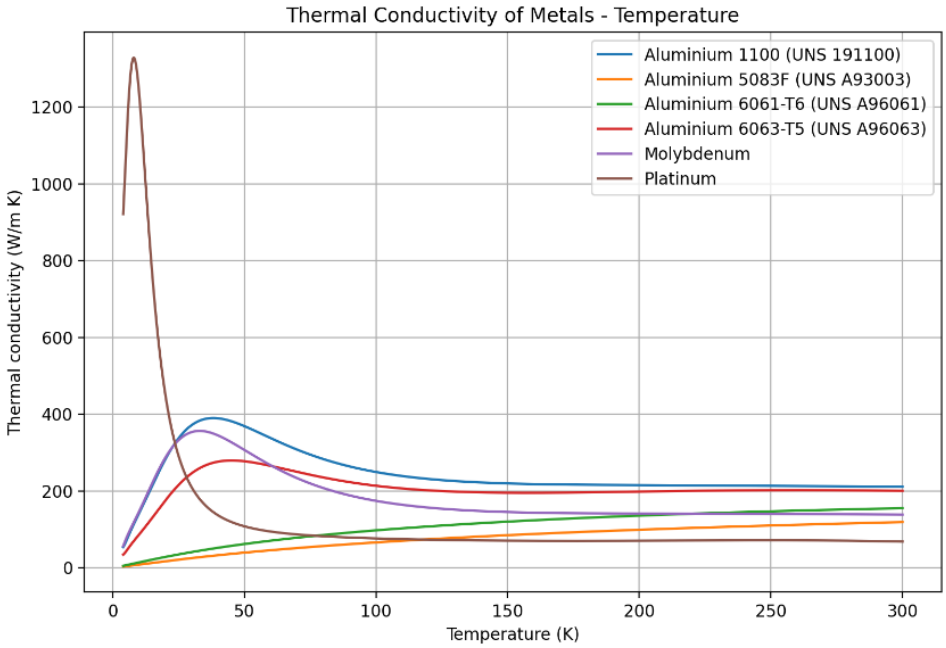

Figure 26: More Thermal Conductivity of metals, data from [18]

Hydrogen embrittlement has a huge impact when steels, titanium or copper are exposed to hydrogen at low temperatures because hydrogen diffuses, and toughness is reduced [19].

Stainless Steel, copper, aluminum, and alloys, due to the face centered cubic crystal structure metals (FCC), have usually good mechanical properties at cryogenic temperatures.

Stainless steel is very common when mechanical properties are important, and the thermal conductivity is a secondary point (from cryogenic materials is the one with the lowest).

Copper, when extremely low temperatures (<100 K) are used, is the material with highest thermal conductivity and above all when talking about high RRR; but has high ductility and easy welding.

Aluminum has very low density (near a third time of the steel's) so when optimizing weight as an achieving point, aluminum is a great option. Furthermore, it has a relatively high thermal conductivity, that is why is used for many cryogenic uses such as heat exchangers or thermal shields. Some 2XXX series (Al-Cu alloys) are stronger than 3XXX, 5XXX and 6XXX, so for specific applications where mechanical properties are extremely important can be used. 3XXX series (Al-Mg alloys) and 6XXX series (Al-Mg-Si alloys) are usually used for heat exchangers, but the 6XXX series has high weldability and better advantages, the most used are the 6061 and 6063 [20].

CHAPTER 5: NUMERICAL MODEL

1 GEOMETRY:

The geometry provided by the Chalmers Department of Mechanics and Maritime Sciences was previously done in the VINK project and the CAD file for the compressor is available [21]. The geometry where the simulations are going to be carried consists of the previously mentioned rotor 3 (R3), stator 3 (S3) and the interconnecting compressor duct (ICD), where the structure vane (STRUT) is located. This part is the intermediate part that connects the high-pressure compressor with the low-pressure compressor.

The next images provide the geometry and the name of each part. The shroud is colored yellow, the hub is colored orange, the blades are colored black, and each of the sides between the next circumferential blade are blue and green.

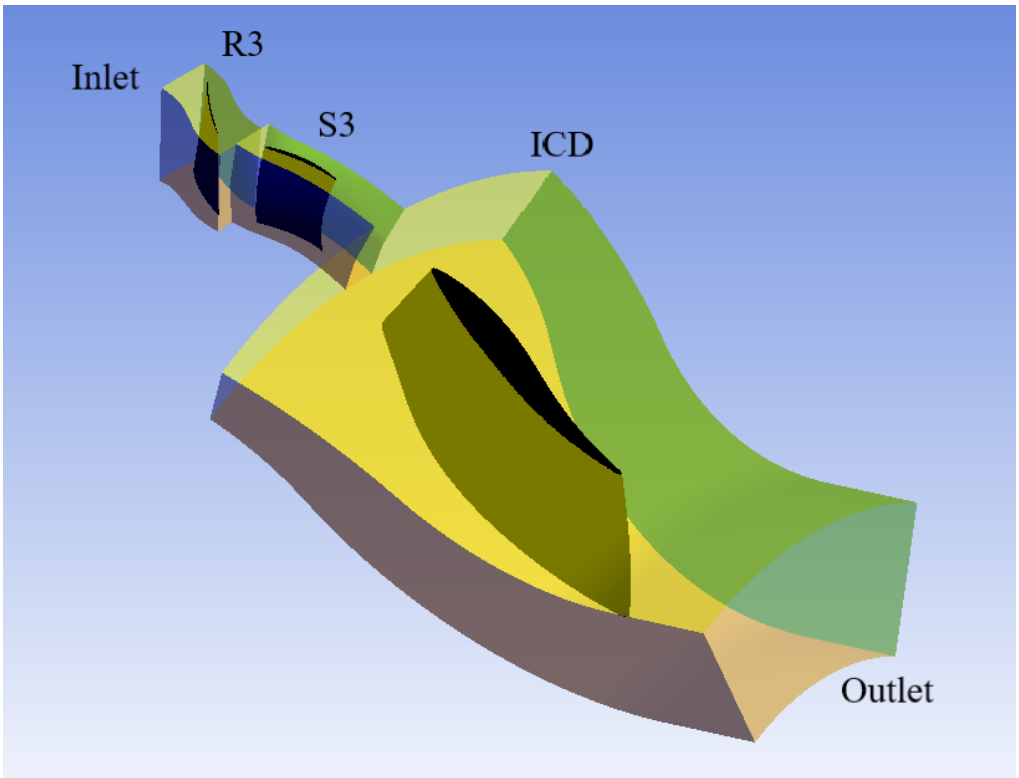

Figure 27: Whole geometry of the package R3, S3 and ICD.

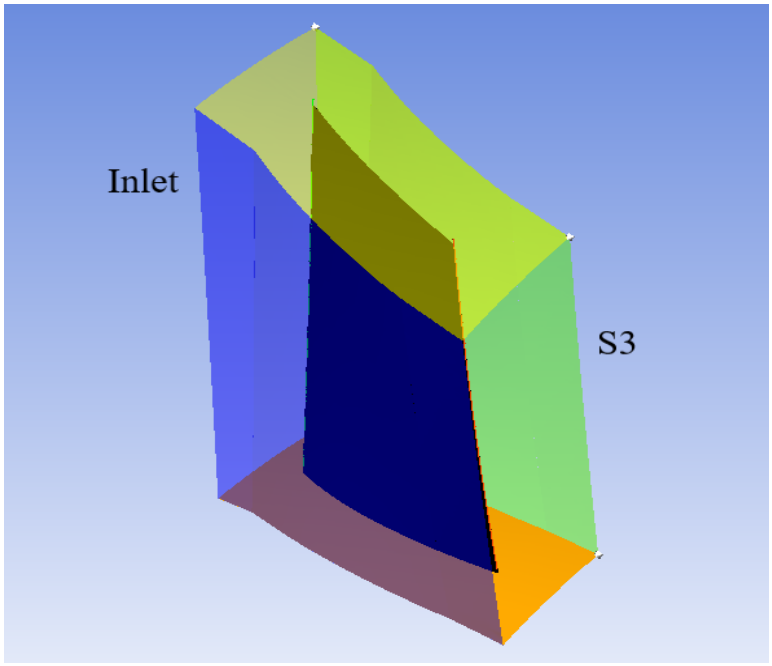

Figure 28: Insight of the R3 geometry.

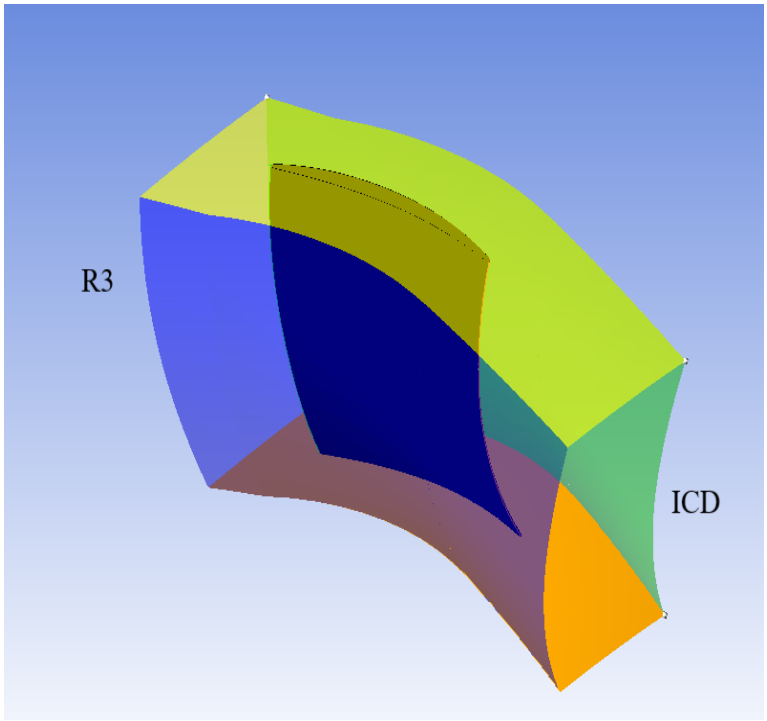

Figure 29: Insight of the S3 geometry.

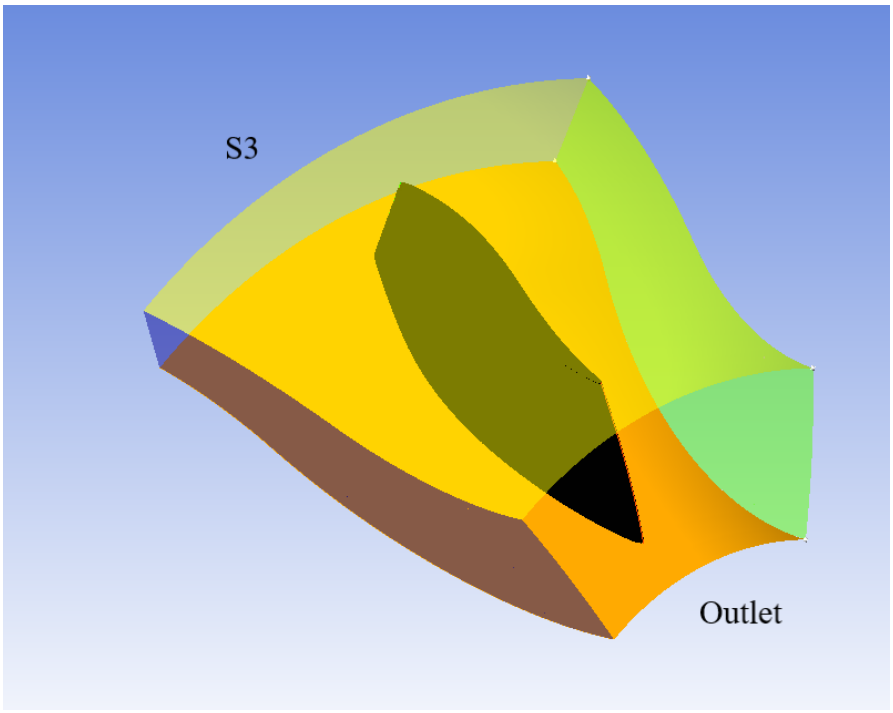

Figure 30: Insight of the ICD geometry.

2 MESH:

The simulations will be run on the engineering simulations software, ANSYS R1 2021 [5]. The desired software to simulate this type of geometry is the turbomachinery blade meshing software, Turbogrid [22]. First, Turbogrid should match what hub, shroud, blade, inlet, outlet and periodics are with the corresponding surfaces. As the focus is the STRUT, the mesh will be specifically focused on that part.

Next, the mesh can be modified in the 'Mesh data' tab. The method of the mesh size can be done by two methods: 'Target Passage Mesh Size', where the number of nodes can be selected among 'Coarse' (20000), 'Medium' (100000), 'Fine' (250000) or 'Specify' (personalized), and 'Global Size Factor', where the overall mesh size is defined and can be increased (not linear) by the 'Size Factor' setting. [23]. The method selected is 'Global Size

Factor' to have a better management and the value will be increased from 1 (less than 1M elements) up to 2 (near 5M elements). Increasing this factor will lead into better accuracy but the simulation time increases exponentially since this rate is not linear, a compromise between accuracy and simulation time is important and will be discussed in the mesh independence study.

Solving the boundary layer is one the most important hits to study the heat transfer and the blade near-wall mesh can be modified in this software in the 'Boundary Layer Refinement Control'. The mesh boundary layer size through the wall changes depending on if its more necessary to be closer or not. The boundary layer thickness depends on the expansion rate (how the layers height one by one increase while separating from the wall), first element offset (the height of the first layer next to the wall) and the number of elements across the boundary layer (the width of the layers).

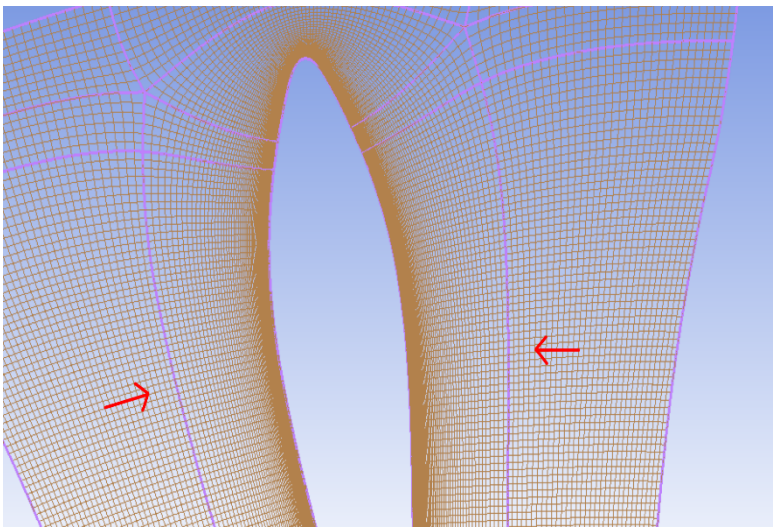

Figure 31: Difference between the boundary layer mesh zone and the different size through the blade wall

The 'Boundary Layer Refinement Control' have two options: 'Proportional to Mesh Size', where the number of elements across the boundary layer is calculated as a relationship of previous and new factors that can be modified like 'Factor Base' and 'Factor Ratio'; and 'First Element Offset' that directly controls the height of the first row of element next to the

blade. The 'First Element Offset' is the one chosen since for achieving $y^+ < 1$ this is the key factor, and the offset will be calculated in section 2.1.

The 'Target Maximum Expansion Rate' tab prevents the expansion rate to get out of the specified maximum rate. In case of selecting the 'First Element Offset', the number of elements across the boundary layer will be increased in order to reduce the maximum expansion rate. This parameter was stated to 1.2 finally by trial-and-error procedure and watching how element number increases and have a compromise.

The 'Near Wall Element Size Specification' control the method by which the near-wall node spacing is specified on the Passage and Hub or Shroud tabs. Can be configured by 'Y plus', that will create a near wall spacing according to a specified Reynolds number, or 'Absolute' that sets the near wall spacing directly. It is used 'Absolute' due to the direct spacing of the wall.

To evaluate the accuracy, mesh variables are analyzed. The next values are for default settings:

-Maximum Face Angle is the maximum angle between two edges of the face that touch the node, measurement of skew and value of 165^o.

-Minimum Face Angle is the minimum angle between two edges of the face that touch the node, measurement of skew and value of 15^o.

-Connectivity Number is the number of elements that touches a node with value of 12.

-Element Volume Ratio is the ratio of the maximum volume of an element that touches a node to the minimum volume of an element that touches a node, measurement of local expansion factor and value of 20.

-Minimum Volume is the minimum volume that an element can have, measurement of that negative volume element is not created and value of 0.

-Edge Length Ratio is the ratio between the longest edge and shortest edge of a face, measurement of aspect ratio and value of 1000.

2.1 CALCULATION OF THE FIRST ELEMENT OFFSET:

Can be calculated by using the equations from the y^+ section and the following expressions [24]:

$$y^+ = \frac{u^* y}{\upsilon} \tag{122}$$

$$u^* = \sqrt{\frac{\tau_w}{\rho}} \tag{123}$$

$$\tau_w = \frac{C_f \rho u_\infty^2}{2} \tag{124}$$

$$C_f = \frac{0.026}{Re_x^{\frac{1}{7}}} \tag{125}$$

$$Re_x = \frac{\rho u_\infty x}{\mu} \tag{126}$$

Where C_f is the skin friction coefficient, u_∞ is the freestream velocity and x the distance from the leading edge (that due to the curvature of the blade and radius depends on the part). The values become from a first simulation to have a first reference of the offset.

$$Re_x = \frac{1.02\ 214\ 0.2}{0.22\ 10^{-5}} = 1.98\ 10^6 \tag{127}$$

$$C_f = \frac{0.026}{Re_x^{\frac{1}{7}}} = \frac{0.027}{1.98\ 10^{6\frac{1}{7}}} = 2.36\ 10^{-3} \tag{128}$$

$$\tau_w = \frac{C_f\ \rho\ u_\infty^2}{2} = \frac{2.36\ 10^{-3}\ 1.02\ 214^2}{2} = 55.06\ \frac{N}{m^2} \tag{129}$$

$$u^* = \sqrt{\frac{\tau_w}{\rho}} = \sqrt{\frac{55.06}{1.02}} = 7.35\ \frac{m}{s} \tag{130}$$

$$y^+ = \frac{u^*\ y}{v} \rightarrow 1 = \frac{7.35\ y}{2.16\ 10^{-5}} \rightarrow y = 2.94\ 10^{-6}\ m \tag{131}$$

After running the simulations with $2.94\ 10^{-6}$, a lower offset was needed to achieve $y^+ < 1$, so the final one is $2.5\ 10^{-7}$.

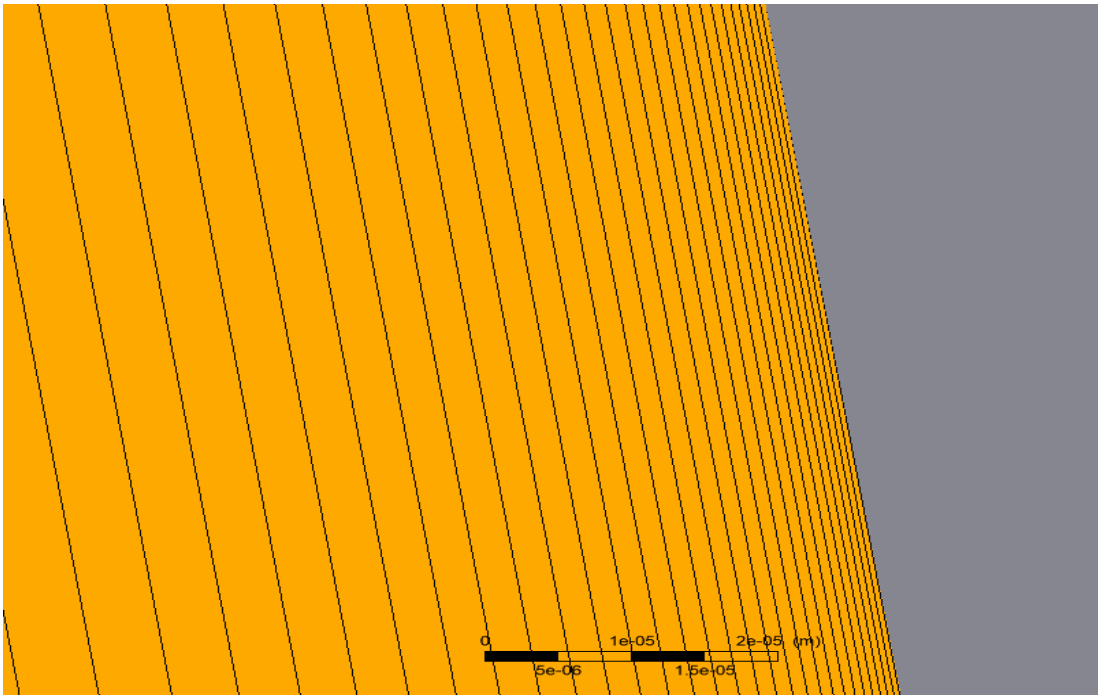

Figure 33: Boundary layer mesh close to the STRUT.

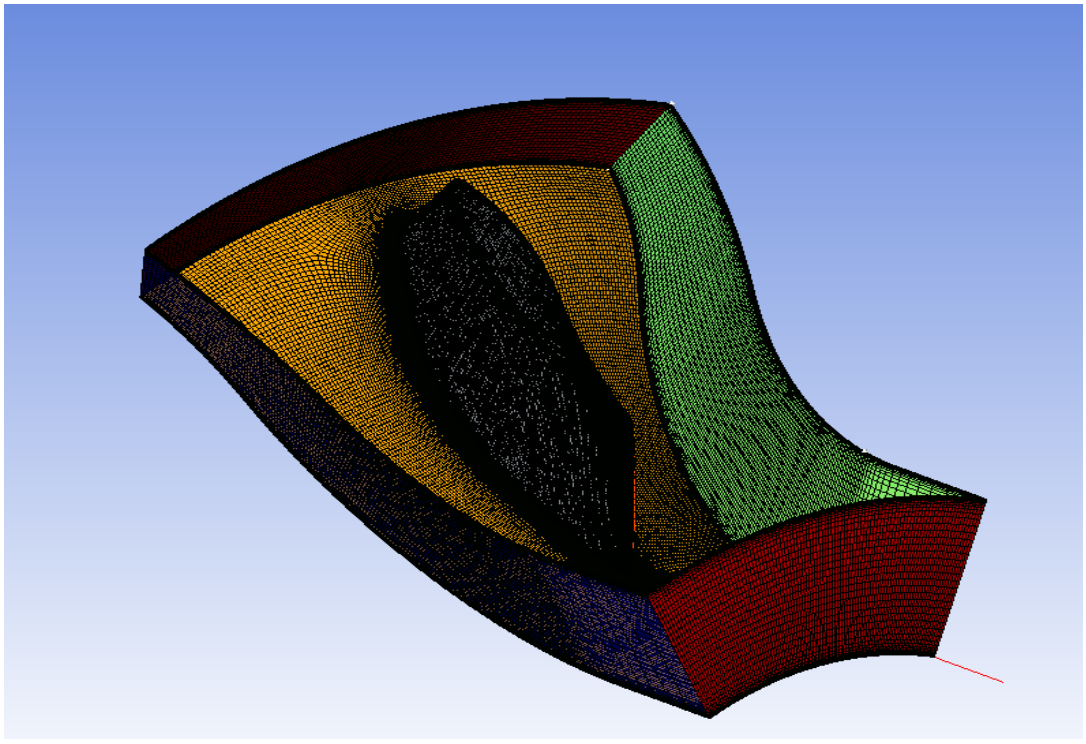

Figure 32: Whole mesh in the ICD except the shroud.

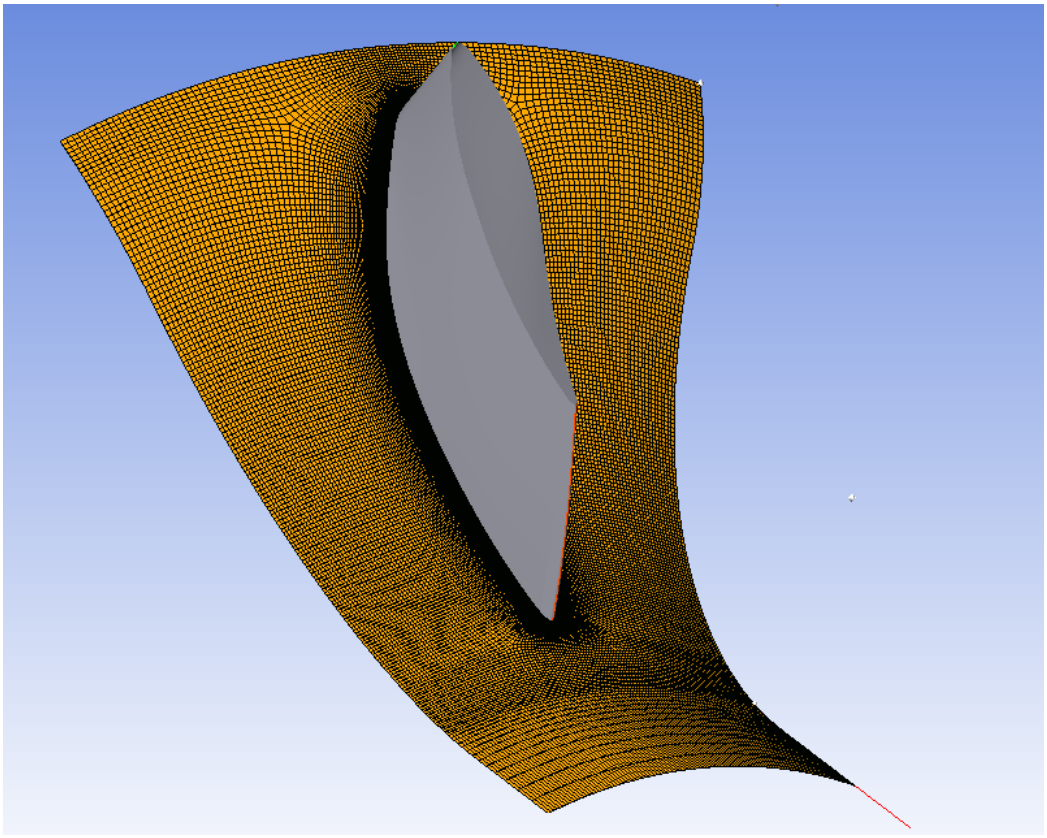

Figure 34: Hub mesh in the ICD

3 SETUP:

After having the geometry and mesh, the next step is to model the fluid that is going to flow through the network and impose characteristics to the walls. For this purpose, CFX-Pre [5] is going to be used.

The material selected is 'Air Ideal Gas' with the next features: The 'Thermodynamic State' is 'Gas', as default. The 'Equation of State' is 'Ideal Gas' (will model de density variation with the ideal gas law) with 'Molas Mass' of 28.96 (kg/kmol), as default. The 'Specific Heat Capacity' is ticked with 'Constant Pressure' option and 1.044 10^3 (J/ kg K), as default. The 'Reference State' tab is activated with 'Reference Temperature' of 25ºC, 'Reference Pressure' of 1 atm, no reference point for enthalpy and entropy, as default. The 'Transport Properties' are one of the most important parts to take in account as explained

before and they are modelled by the 'Sutherlands Formula'. The 'Radiation Properties' are activated with the default settings.

The domain parts, R3, S3 and ICD, have 'Domain Type' as 'Fluid Domain' since is where the fluid flow. The material selected is previously modelled 'Air Ideal Gas' with 'Morphology of 'Continuous Fluid'. The 'Reference Pressure' is 0 atm, 'Non Buoyant' because its it depreciable, 'Domain Motion' as 'Stationary' and no 'Mesh Deformation'. In the 'Fluid Models' tab there are several 'Heat Transfer' options: 'Isothermal' is used to evaluate fluid properties dependency with temperature, 'Thermal Energy' is the same as 'Total Energy' neglecting kinetic energy effects, 'Total Energy' models enthalpy and kinetic energy effects. This last one is the one used because uses the mathematical model explained before. The 'Viscous Work Term' is included because involves Total Energy equation. [25] The 'Turbulence' model used is the 'Shear Stress Transport' (SST) and when transition is modelled, the 'Gamma Theta Model' is used. Combustion and thermal radiation are not clicked. 'Initialization' is not used.

For surfaces there are 5 types of boundary conditions: 'Inlet' (the flow goes into the domain), 'Outlet' (the flow goes outside the domain), 'Opening' (mix of the previous where the flow can go inside or outside), 'Wall' (the flow collides because is an impermeable wall and heat transfer can happen) and 'Interface' (the flow is symmetrical to a plane). The hub, shroud and blades are 'Wall'; the ICD outlet is 'Outlet'; the R3 inlet is 'Inlet'; the rest of the surfaces are "not real" (as the inlet and outlet) and are interfaces among them or symmetric between the adjacent blades.

The inlet and outlet conditions were stated in previous simulations or guessed design point. The inlet conditions are introduced by a csv file and imposing 'Static Frame Total Pressure', 'Flow Direction', 'Turbulence' as 'Medium', and 'Static Frame Total Pressure'. The outlet conditions are 'Average Static Pressure' to 106810 Pa with a profile of 0.05 'Average Over Whole Outlet'.

Walls (except the STRUT vane) are defined as 'No Slip Wall' in 'Mas And Momentum' due to this option makes fluid velocity the same as the wall velocity, 'Smooth

Wall' in 'Wall Roughness', and 'Heat Transfer' as 'Adiabatic' (no heat transfer) because a boundary condition may be introduced to enable heat transfer to be computed. In the STRUT, where the heat transfer is studied, the 'Heat Transfer' boundary condition can be stated to 'Adiabatic', 'Temperature', 'Heat Flux' or 'Heat Transfer Coefficient'. The boundary conditions will be obtained from a first calculation with the heat transfer theory. Will be set to 'Temperature' at 91K.

The solver control is the same as default with the option of 'High Resolution' to enforce a boundedness criterion.

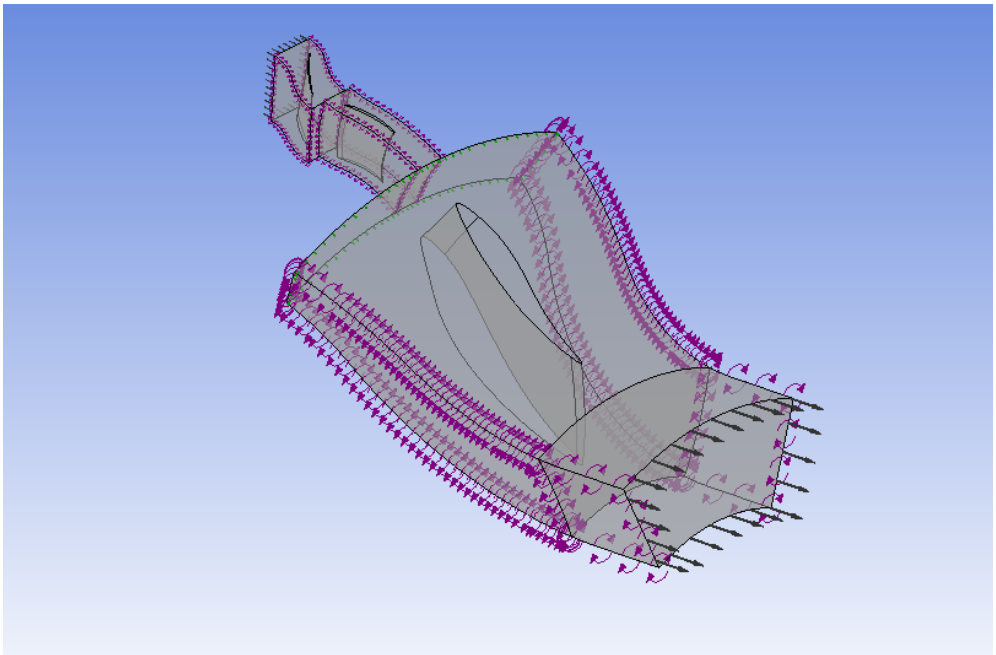

Figure 35: Setup network.

3.1 BOUNDARY CONDITION ESTIMATION:

Air is flowing through the ICD, which is the hot fluid, inside the STRUT there is Hydrogen (H_2) flowing to refrigerate, cold fluid, and the thickness of the vane is not well-defined yet, but it will be assumed 5% of the total width that is approximately $0.002\ m$.

The air properties are estimated from a first simulation of the case and the variation between the properties and other variables relevant for this first study at the first and sequent simulations are so low. The correlations given before for flat plate needs the fluid's properties at the film temperature at the ICD inlet (when using the correction factor, they might be evaluated at the freestream temperature). Most of the relevant properties are displayed in the Table 2.

$$T_{film} = \frac{T_{freestream} + T_{wall}}{2} \tag{132}$$

$Freestream\ temperature\ (T_\infty)$	$371\ K$
$Film\ temperature\ (T_{film})$	$230\ K$
$Freestream\ Mach\ number\ (Ma_\infty)$	0.70
$Freestream\ pressure\ (p_\infty)$	$110172\ Pa$
$Film\ density\ (\rho_\infty)$	$1.66\ \frac{kg}{m^3}$
$Freestream\ velocity\ (u_\infty)$	$203\ \frac{m}{s}$
$Film\ dynamic\ viscosity\ (\mu_{film})$	$1.50\ 10^{-5}\ kg/m\ s$
$Film\ Prandtl\ number\ (Pr_{film})$	0.72
$Film\ thermal\ conductivity\ (k_{film})$	$0.02\ W/m\ K$

Table 2: ICD Air Inlet conditions

The material used for vane is guessed Aluminum 6063 with a thermal conductivity at $91\ K$ of approximately $237\ W/m\ K$. As the thickness is extremely small, variations on

the vane's thermal conductivity leads on a small difference (having an increase of 100 %, will lead just on a difference of 2 K) so aluminum is a good reference since this series has also good mechanical properties.

The hydrogen will be flowing inside the STRUT and as is a still developing part of the whole project, will be assumed a temperature and the consequent properties are displayed below. The pressure is the estimated after the pump from the Department.

$Temperature\ (T)$	$27\ K$
$Hidraulic\ diameter\ (D_h)$	$0.002\ m$
$Pressure\ (p)$	$40\ 10^5\ Pa$
$Density\ (\rho)$	$68.60\ \frac{kg}{m^3}$
$Velocity\ (u)$	$1\ \frac{m}{s}$
$Dynamic\ viscosity\ (\mu)$	$1.12\ 10^{-5}\ kg/m\ s$
$Prandtl\ number\ (Pr)$	1.14
$Thermal\ conductivity\ (k)$	$0.011\ W/m\ K$

Table 3: Hydrogen properties

To start this problem, a wall temperature (T_{wall}) must be guessed and calculate the heat flux. After, a new wall temperature will come up. To solve the one-dimensional problem, iteration is needed substituting the new wall temperature each time until it does not change significantly. Finally, a wall temperature of 91 K was stated.

CHAPTER 6: RESULTS

1 *FULLY TURBULENT ICD SIMULATIONS:*

As said before, the finer mesh is it, better accuracy for the problem; but there must be a compromise between accuracy and solving time. The boundary layer offset ('First Element Offset') must the same in all the simulations because it allows to define the boundary layer. This accuracy is dependent on how fine the mesh is, and this property can be varied with the 'Global Size Factor', and it will be varied between 1 (less than 1M elements that can be run in 2 hours) and 2 (near 5M elements that can take up to 16 hours to have a reasonable convergence). A mesh independence study will be done by comparing the heat transfer coefficient over the STRUT with different number of elements until the variation is assumable.

For the first simulation, 'Global Size Factor' of 1.25 was selected to have 1257001 elements and an average heat transfer coefficient of 725 $W/m^2\,K$. For the second one, a 'Global Size Factor' of 1.65 to achieve 2467608 elements and an average heat transfer coefficient of 733 $W/m^2\,K$. Finally, with a 'Global Size Factor' of 2, up to 4758722 elements were created to compute an average heat transfer coefficient of 734 $W/m^2\,K$; where the difference is so low. The number of elements previously mentioned correspond to only the ICD mesh.

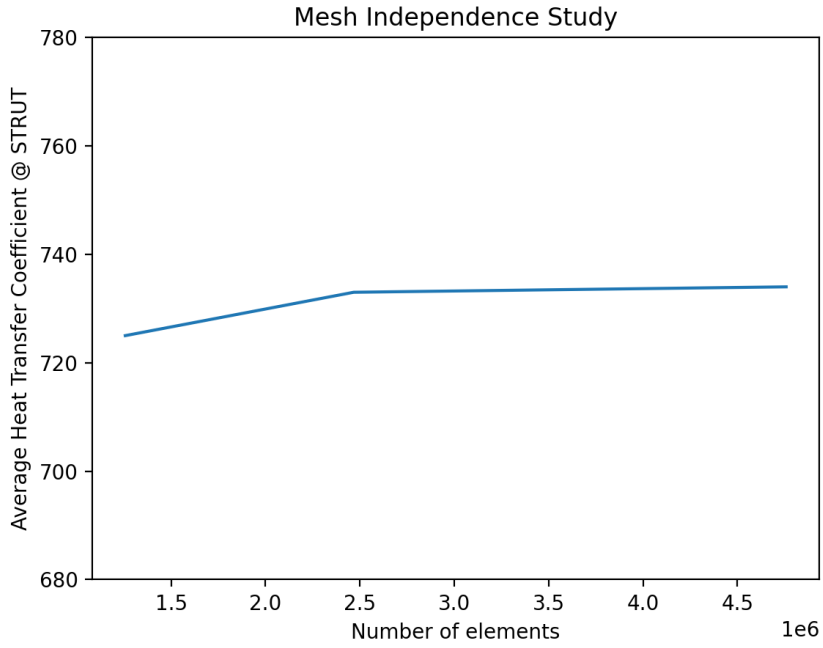

Figure 36: Mesh Independence Study of the fully turbulent ICD case.

The y^+ value around the STRUT is wherever below 1. The most critical part is the leading edge. When the wall temperature is changed for higher values, the maximum y^+ value goes lower up to 50% difference (below 0.5) because the variation of the properties for very low temperatures in comparison with higher ones, leads on higher heat transfer coefficients and boundary layer is more aggressive. The y^+ value can be plotted by adding a 'Contour' and selecting where and what variable is desirable to plot over a surface. The software already recognizes this variable.

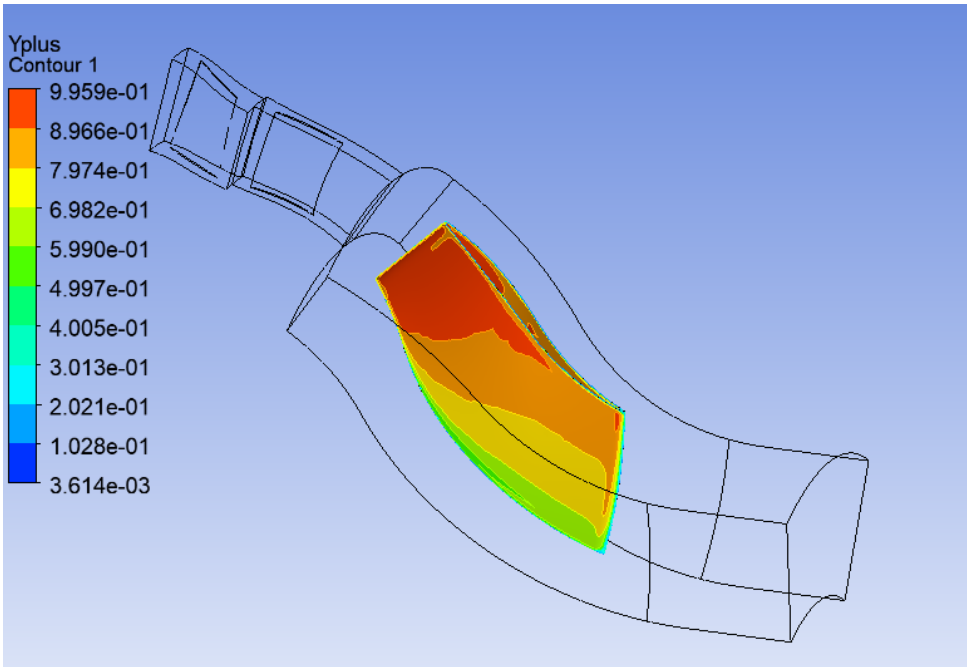

Figure 37: y+ value over the STRUT with fully turbulent flow and 91K wall temperature.

Ansys CFX computes the 'Wall Heat transfer Coefficient' from a "Wall Adjacent Temperature" (T_{nw}) that is the average temperature in the first element adjacent to the wall, not from the fluid's temperature as seen in Equation 7. The heat transfer from a fixed temperature reference is stated in CFX for laminar flow as [13]:

$$q_w = h_c\,(T_w - T_{nw}) \tag{133}$$

For turbulent flow as:

$$q_w = \frac{\tau_w\, c_p}{Pr_t\, U}\left(T_w - T_f - \frac{Pr_t\, U^2}{2\, c_p}\right) \tag{134}$$

With viscous work active:

$$T_{nw} = T_f + \frac{Pr_t\, U^2}{2\, c_p} \tag{135}$$

This leads on having very high values for the default 'Wall Heat Transfer Coefficient", but this can be avoided by 2 ways.

First, making an expert parameter. In CFX-Pre, in the 'Solver' tab, by right-clicking, an 'Expert Parameter' can be added. In the 'Physical Models' tab, the bulk temperature can be added in 'tbulk for htc' and the heat transfer coefficient will be calculated taking in account this temperature specified.

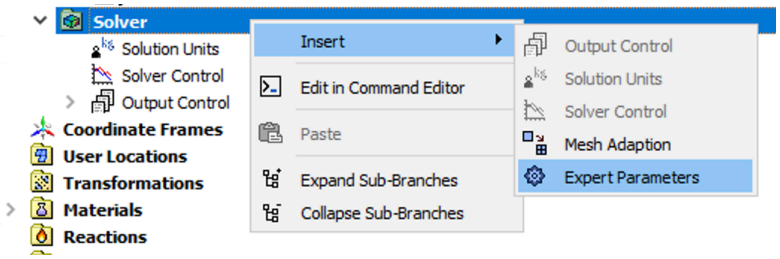

Figure 38: Expert parameter selection in CFX-Pre.

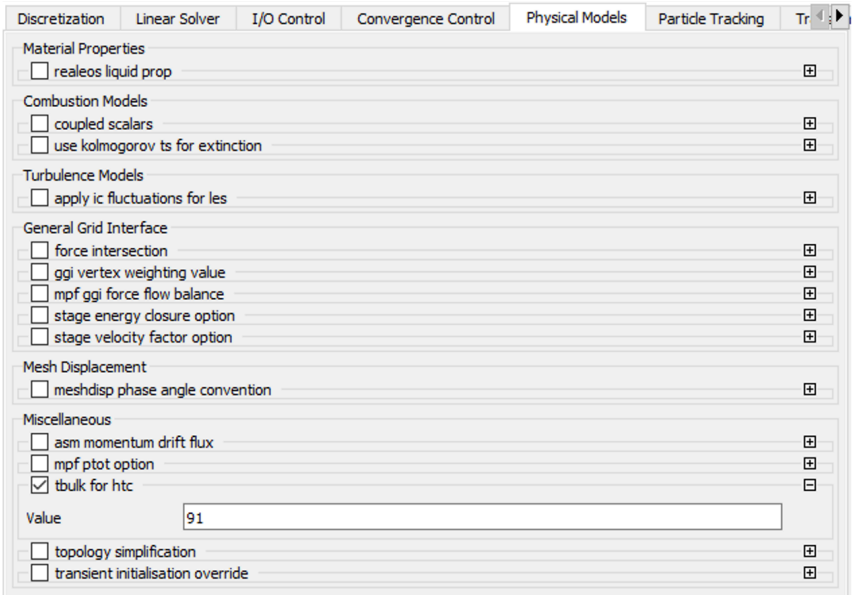

Figure 39: 'tbulk for htc' selection in CFX-Pre.

Second, work with the 'Wall Heat Flux' variable. Since the energy is conserved, the heat flux will be the same even if the calculation of the heat transfer coefficient is different. In CFX-Post, expressions and a consequently linked variable (making sure that does not have the same name) can be created. The following equation defines this relation:

$$HTC = areaAve\ (Wall\ Heat\ Flux)\ @\ ics\ Blade\ /\ (areaAve(Temperature)\ @\ ics\ Blade - massFlowAve\ (Temperature)@\ ics\ to\ s3\ Side\ 1 \quad (136)$$

Where $areaAve$ does the average depending on the area surface of the variable specified in parenthesis over the surface specified after the @, $massFlowAve$ does the average over a surface but depending on the local mass flow, $ics\ to\ s3\ Side\ 1$ is the surface connecting the ICD and the S3, and thereby, the $massFlowAve$ can only be used in surfaces where fluid flows.

This option is desirable because for the previous method, a 'tbluk for htc' should be specified before each simulation, so if when the simulation is already run, this temperature varies, the heat transfer coefficient will vary.

The heat transfer coefficient over the STRUT can be plotted by using the Equation 136 without $areaAve\ (Wall\ Heat\ Flux)$ to have the local heat transfer coefficient.

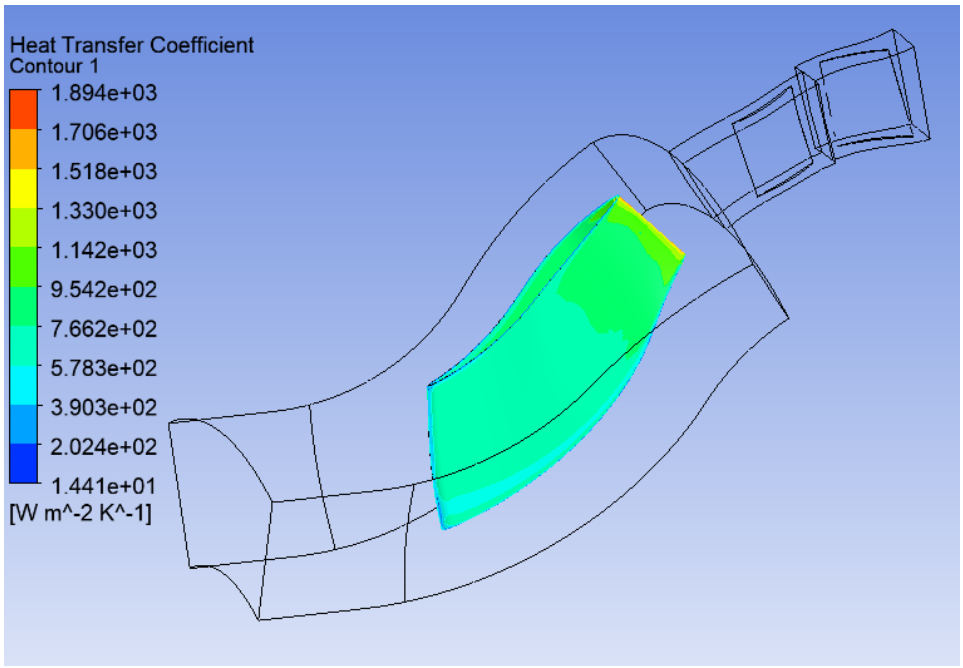

Figure 40: Heat Transfer Coefficient over the STRUT with fully turbulent flow.

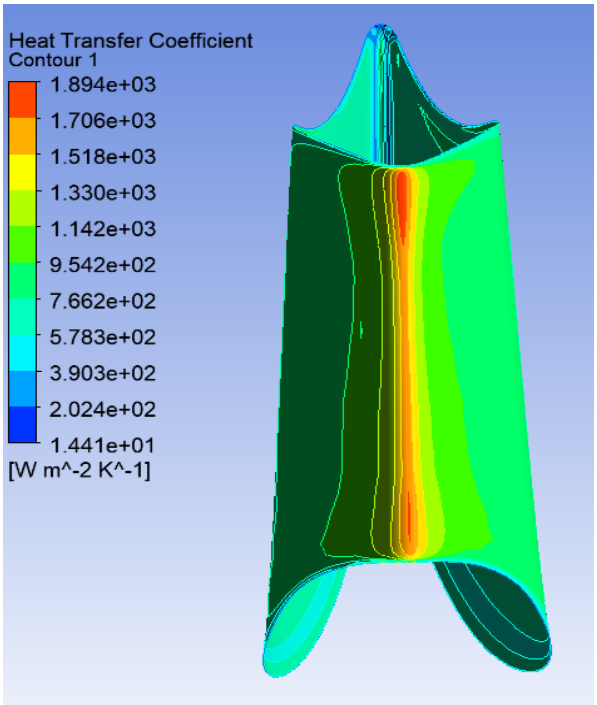

Figure 41: Insight of the heat transfer coefficient in the STRUT leading edge with fully turbulent flow.

From the 'Turbo' tab, plots referring to the blade geometry are easy to do with different configurations: 'Blade Loading', 'Circumferential', 'Hub to Shroud' and 'Inlet to Outlet'. 'Blade Loading' allows to plot variables over the blade streamwise normalized (0,1) at different span. The span selected is 0.5 as is the midterm value. Both sides of the blade are represented in Figure 37, that is why it looks doubled. When reaching 0.95 spanwise, there is a sudden peak and immediately it drops, this could be related with a separation of the flow from the wall because in the last part, where this happens, is no longer similar to a flat plate and it is more likely to the flow through a ball, where near the second half, the flow separates due to the aggressive roundness and cannot follow the shape.

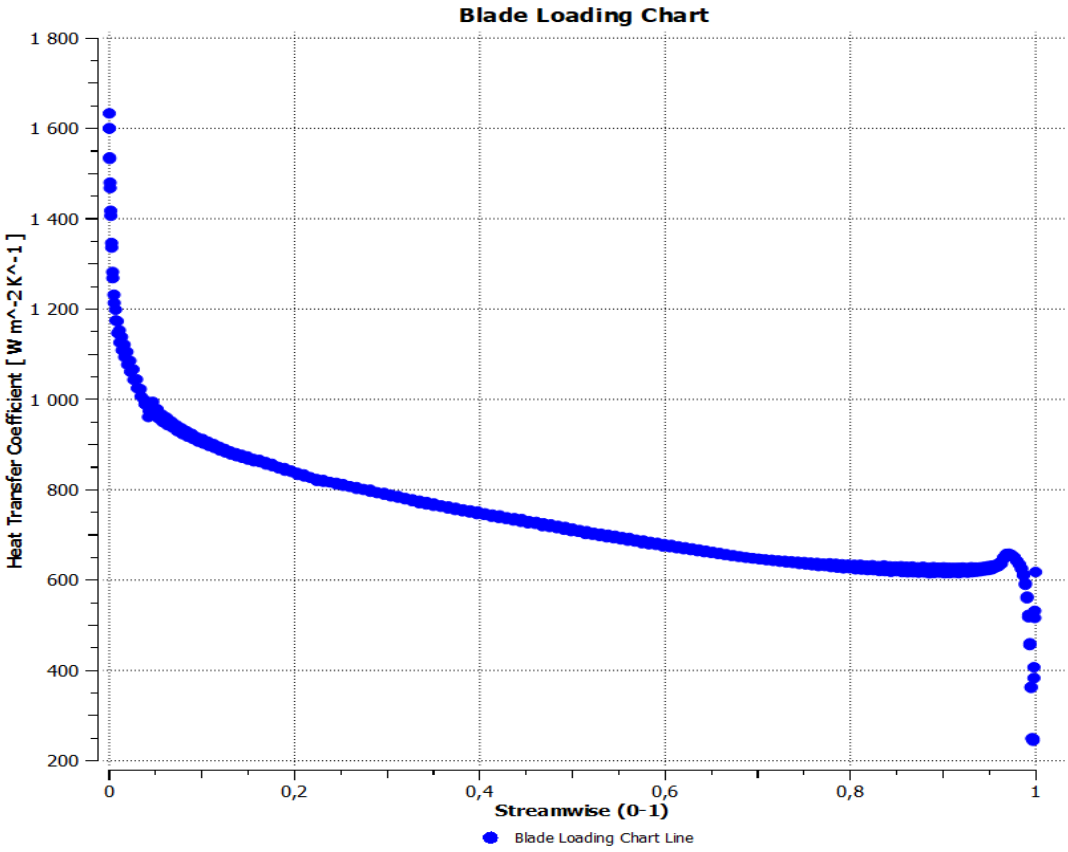

Figure 42: Heat transfer coefficient streamwise at 0.5 span in the STRUT with fully turbulent model.

This local heat transfer coefficient from the simulation is compared with the local heat transfer coefficient from the flat plate verification and from the correlations. For the flat plate it is used a simple domain of a flat plate with the same boundary conditions at the inlet and outlet of the ICD, leading a closer and simpler case but taking in account that the blade is a mid-term geometry of the flat plate and a cylinder. It is also used the recommendation of evaluate the properties at the freestream temperature and multiply the final result by the correction factor $(T_w / T_\infty)^{-n}$, trying different exponents.

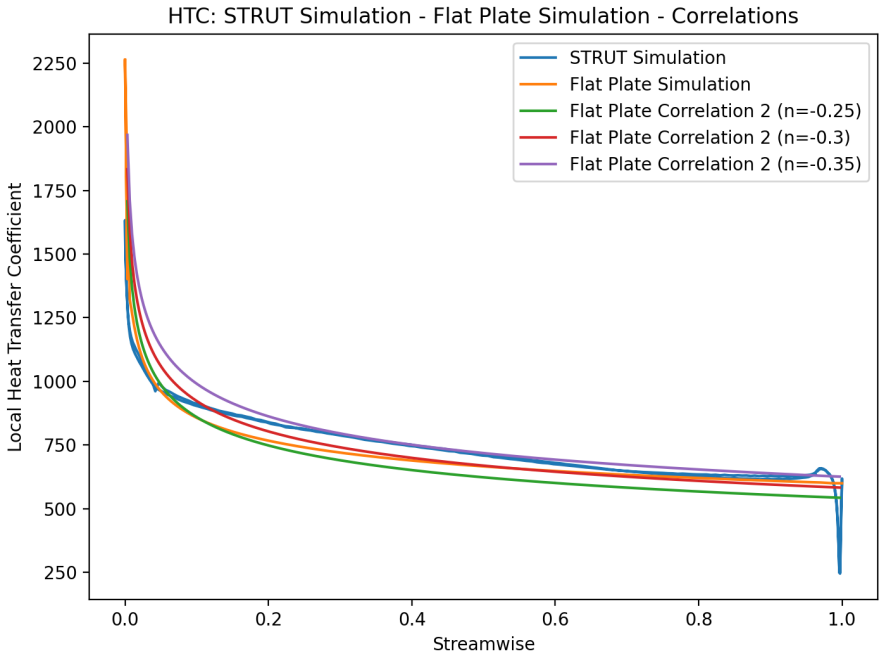

Figure 43: Comparison in the fully turbulent model of the heat transfer coefficient from the whole package simulation, flat plate simulation and correlations.

One of the most interesting parts to study and treat in this project is the influence of the huge temperature variation of the flow. To show the importance of this factor in the problem, further heat transfer coefficient comparison is done comparing the main case with variable properties, with constant properties (except density that is modeled by ideal gas theory) at $25^{o}C$ and 1 atm such as dynamic viscosity and thermal conductivity with values of $1.831\ 10^{-5}\ kg/m\ s$ and $0.0261\ W/m\ K$ respectively.

The average heat transfer coefficient on the STRUT was stated before as $734\ W/m^2\ K$ and for the previously described case rises up to $880\ W/m^2\ K$, an increase of 19.89 % that is avoided due to the correct configuration.

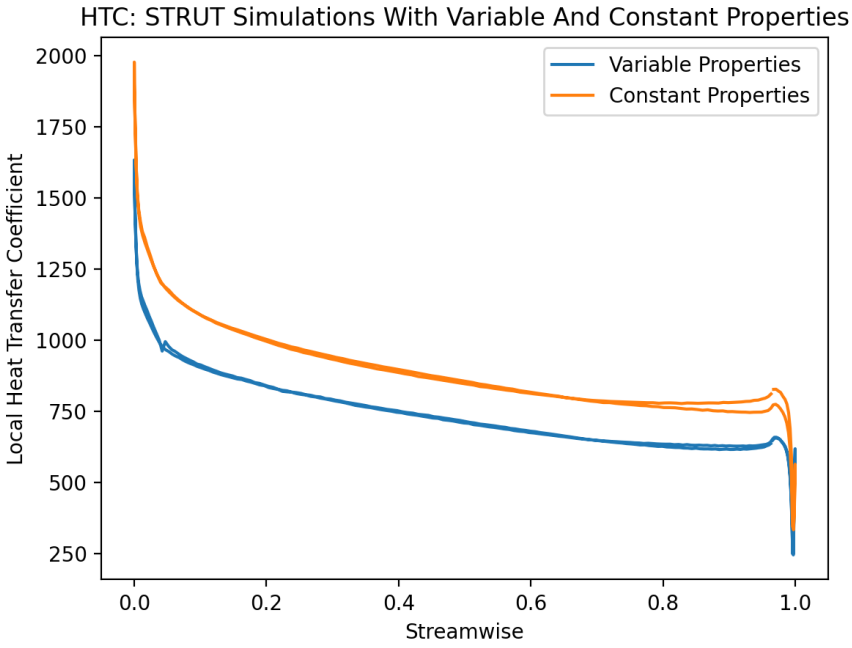

Figure 44: STRUT Simulations With Variable And Constant Properties.

Another comparison is done by simulating the main configuration with different wall temperatures. Remembering that with 91 K there is an average heat transfer coefficient of 734 $W/m^2\,K$; for 120 K is 722 $W/m^2\,K$, for 140 K is 708 $W/m^2\,K$, for 160 K is 695 $W/m^2\,K$ and for 200 K is 672 $W/m^2\,K$. Up to a limit, decreasing the wall temperature leads on having less heat transfer.

In conclusion, the model predicts quite well the phenomena if the desired n exponent is -0.35 that is in the provided range. Other factors are shown to exalt the relevance of it, such as the huge variation of the heat transfer without taken in account the variable properties or the different wall temperature.

2 *TRANSITION ICD SIMULATIONS:*

After simulating, comparing, and verifying the fully turbulent model, an insight on the laminar and transition region is done. More steps were explained in the previous section but this one is more straightforward as there is information recovered from the preceding. The simulation is run with the 'Global Size Factor' of 2 configuration and applying to the fluid model in the 'Transitional Turbulence' tab the 'Gamma Theta Model'.

The average heat transfer coefficient over the STRUT vane is $723.713\ W/m^2\ K$, in the flat plate model is $655.227\ W/m^2\ K$, and the correlations leads $675.01\ W/m^2\ K$ for $n = -0.25$, $704.64\ W/m^2\ K$ for $n = -0.3$, and $757.62\ W/m^2\ K$ for $n = -0.35$. A plot of the local heat transfer coefficient is provided in Figure 46.

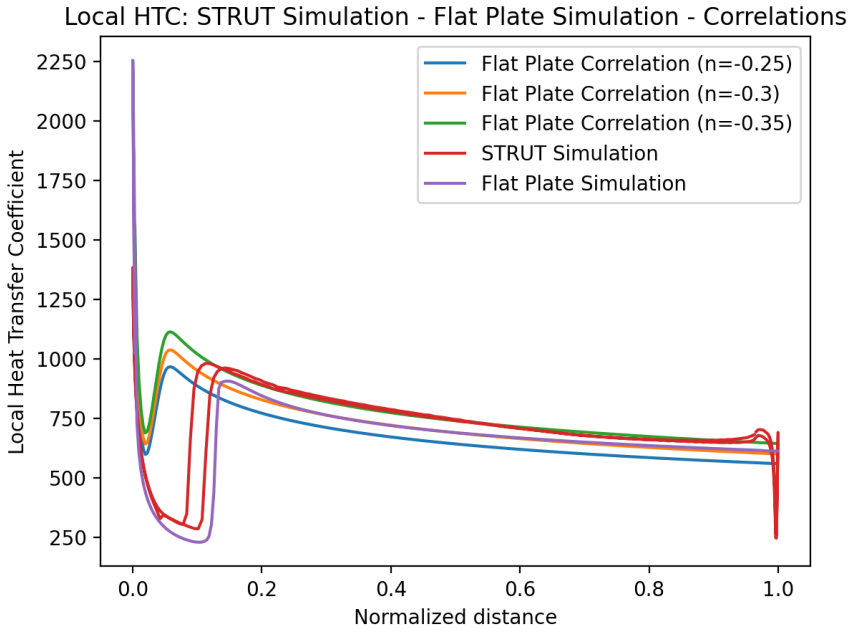

Figure 45: Comparison of the transition model of the heat transfer coefficient from the whole package simulation, flat plate simulation and correlations.

In contrast with the fully turbulent model, the transition model differs significantly from the correlations even in the flat plate. The most significant changes are the onset Reynolds number, that marks when the transition occurs and thereby is a huge difference because the correlations for the inlet turbulent intensity predicts a minimum laminar region, and the length of the transition region, that the simulations predict a very vanish region. Even in both simulations there is a huge difference of heat transfer coefficient in the turbulent region, where should be practically superimposed as in the fully turbulent model; obviously this offset results in an offset in the average heat transfer coefficient.

CHAPTER 7: CONCLUSION

An explanation on how to perform a heat transfer study has been done. First, looking to the actual turbulence models. Second, validate them. Finally, making the desired simulations. Throw all this parts, an explanation was done above all ANSYS configuration as they were researched for this purpose.

The fully turbulent model is accurate for this purpose and in addition, the correlations validate it very well with a deviation of 3%.

Reaching the transition model, the flat plate verification did not accurately predict the transition region. In fact, did not achieve the onset Reynolds number that is one of the most important parameters on the transition. The onset Reynolds number is only dependent on the inlet turbulence intensity, that is not function of fluid properties that can vary with temperature, like other parameters as the Nusselt number. It is important to highlight that the turbulence intensity used is the one at the ICD inlet, not at the STRUT start, so there may be a decay between these two points that leads on a lower turbulence intensity and thereby an approximation between the simulations and the correlations. In addition, as the laminar region is much higher in the simulations (and the heat transfer coefficient is lower in this region), this value becomes lower, with a difference of 7.5%.

The transition model is not accurate, but a further conclusion can be done. Under the assumption that the correlations from the previous papers mentioned and validated with experimental data are correct, the equations predict an extremely small laminar region and both correlations and simulations (even if are not correct) also predict a rapid transition. For this case, the approximation for heat transfer of having a fully turbulent model could be taken as the transition model used does not predict it, but the deviation from the fully turbulent model is of 4%.

Further development can be done on using the present Thesis to compute the heat transfer coefficient over the hub and shroud. New transition models should be tried to compute the real laminar and transition region of the STRUT or do experimental studies to develop more accurate correlations for high temperature differences.

CHAPTER 8: BIBLIOGRAPHY

[1] ENABLE2 Project. https://www.enableh2.eu/ .

[2] European Green Deal, December 2019, https://ec.europa.eu/clima/policies/strategies/2050_en

[3] Isak Jonsson, Carlos Xisto, Hamidreza Abedi, Tomas Grönstedt, Marcus Lejon, "FEASIBILITY STUDY OF A RADICAL VANE-INTEGRATED HEAT EXCHANGER FOR TURBOFAN ENGINE APPLICATIONS", June 2020, London.

[4] Long-Gang Liu, Xue-Song Li, Xiao-Dong Ren and Chun-Wei Gu, "Investigation of Cooling Effect on the Aerodynamic Performance in the Intercooled Compressor", July-August 2018, People's Republic of China.

[5] Ansys CFX: Turbomachinery CFD Software: https://www.ansys.com/products/fluids/ansys-cfx

[6] MathWorks MATLAB: https://es.mathworks.com/products/matlab.html

[7] Python: https://www.python.org/

[8] Theodore L Bergman, Adrienne S. Lavine, Frank P. Incropera, David P. Dewitt, "FUNDAMENTALS OF HEAT and MASS TRANSFER", Seventh Edition.

[9] Randall F.Barron, Gregory F.Nells, "Cryogenic heat transfer", Second Edition.

[10] F.M. White, "Viscous Fluid Flow", 3rd ed., McGraw-Hill, 2006.

[11] https://www.nuclear-power.com/nuclear-engineering/heat-transfer/convection-convective-heat-transfer/laminar-vs-turbulent-nusselt-number/

[12] John H. Lienhard V, "Heat Transfer in Flat-Plate Boundary Layers: A correlation for Laminar, Transitional, and Turbulent Flow", June 2020.

[13] CFX-Solver Modeling Guide, https://ansyshelp.ansys.com/account/secured?returnurl=/Views/Secured/corp/v211/en/cfx_mod/cfx_mod.htlm

[14] Ian H. Bell, Jorrit Wronski, Sylvain Quoilin and Vincent Lemort, "Pure and Pseudo-pure Fluid Thermophysical Property Evaluation and the Open-Source Thermophysical Property Library CoolProp", https://pubs.acs.org/doi/abs/10.1021/ie4033999

[15] Jonas Bredberg, "On the Wall Boundary Condition for Turbulence Models", 2000, Chalmers University of Technology.

[16] H. Tennekes and J. L. Lumley, "A first Course in Turbulence. Massachusetts Intitute of Techology", Cambridge, 1976.

[17] P. Duthil, "Material properties at Low Temperature", Institut de Physique Nucléaire d'Orsay.

[18] National Institute of Standars and Technology U.S. Department of Commerce, https://trc.nist.gov/cryogenics/index.html

[19] Harry Bhadhesia, "Prevention of Hydrogen Embrittlement in Steels", December 2020, Cambridge University.

[20] Jaroslaw Polinski, "Materials in cryogencs", European Course in Cryogenics 2010, Geneva.

[21] VINK Compressor, https://github.com/nikander/VINK

[22] Ansys TurboGrid: Turbomachinery Blade Meshing Software, https://www.ansys.com/products/fluids/ansys-turbogrid

[23] ANSYS TurboGrid User's Guide, https://ansyshelp.ansys.com/account/secured?returnurl=/Views/Secured/corp/v211/en/tg_user/tg_user.htlm

[24] Frank M. White, "FLUID MECHANICS", Seventh Edition.

[25] CFX-Pre User's Guide, https://ansyshelp.ansys.com/account/secured?returnurl=/Views/Secured/corp/v211/en/cfx_pre/cfx_pre.htlm

[26] Reynolds, Osborne, "On the Dynamical theory of Incompressible Viscous Fluids and the Determination of the Criterion", 1895.

[27] Boussinesq, Joseph (1903), "Thōrie analytique de la chaleur mise en harmonie avec la thermodynamique et avec la thōrie mc̄anique de la lumi_re: Refroidissement et c̄hauffement par rayonnement, conductibilit ̄des tiges, lames et masses cristallines, courants de convection, thōrie mc̄anique de la lumi_re", 1903.

[28] Launder, B.E., Spalding D.B., "The numerical computation of turbulent flows", 1974.

[29] Wilcox, D.C., "Formulation of the k-ω Turbulence Model Revisited", 2008.

[30] R.B. Langtry, "A Correlation-Based Transition Model using Local Variables for Unstructured Parallelized CFD Code", 2006.

[31] Pointwise, https://www.pointwise.com/ .

[32] Menter, F.R., "Two-Equation Eddy-Viscosity Turbulence Models for Engineering Applications", August 1994.